

Brownian Gaussian Unitary Ensemble: non-equilibrium dynamics, efficient k -design and application in classical shadow tomography

Haifeng Tang^{a,b}

^a*Department of Physics, Stanford University, Stanford, California 94305, USA*

^b*Stanford Institute for Theoretical Physics, Stanford University, Stanford, California 94305, U.S.A.*

E-mail: hftang@stanford.edu

ABSTRACT: We construct and extensively study a Brownian generalization of the Gaussian Unitary Ensemble (BGUE). Our analysis begins with the non-equilibrium dynamics of BGUE, where we derive explicit analytical expressions for various one-replica and two-replica variables at finite N and t . These variables include the spectral form factor and its fluctuation, the two-point function and its fluctuation, out-of-time-order correlators (OTOC), the second Rényi entropy, and the frame potential for unitary 2-designs. We discuss the implications of these results for hyperfast scrambling, emergence of temperature, and replica-wormhole-like contributions in BGUE. Next, we investigate the low-energy physics of the effective Hamiltonian for an arbitrarily number of replicas, deriving long-time results for the frame potential. We conclude that the time required for the BGUE ensemble to reach k -design is linear in k , consistent with previous findings in Brownian SYK models. Finally, we apply the BGUE model to the task of classical shadow tomography, deriving analytical results for the shadow norm and identifying an optimal time that minimizes the shadow norm, analogous to the optimal circuit depth in shallow-circuit shadow tomography.

KEYWORDS: Brownian GUE, hyper-fast scrambling, temperature, replica wormhole, complexity, efficient k -design, classical shadow tomography

Contents

1	Introduction	1
2	Non-equilibrium dynamics: exact results for one/two-replica variables	3
2.1	Averaged evolution operator on one and two replica space	4
2.2	One-replica observables	8
2.3	Two-replica observables	9
3	Approaching k-design for arbitrarily many replicas	14
3.1	Low energy spectrum	14
3.1.1	Ground states	14
3.1.2	First excited states	16
3.1.3	Second excited states	18
3.1.4	General excited states in the infinite N limit	21
3.2	Approaching k -design	21
4	Application in classical shadow tomography	22
4.1	Brief review of classical shadow tomography	22
4.2	Classical shadow tomography using BGUE	24
5	Conclusion	26
A	Subset of High Energy Spectrum	27

1 Introduction

Motivation In recent work by Chen et al. [1], an efficient approximation of a k -design of the Haar random unitary ensemble was explored using an $N \times N$ Hamiltonian H drawn from the Gaussian Unitary Ensemble (GUE) [2]. Due to energy conservation, $U_t = e^{iHt}$ cannot approach a k -design until a parametrically long time, which scales with some power of N [3, 4]. To overcome this obstacle, the authors proposed splitting the evolution into two ranges, where the system evolves under different GUE Hamiltonians in each range. Specifically, they considered the construction $U_t = e^{iH_1 t/2} e^{iH_2 t/2}$, where H_1 and H_2 are independently drawn from GUE. A key feature of this approach is that H_1 and H_2 generally do not commute, causing the spectrum of U_t to mix quickly and distribute uniformly on the unit circle. This suggests that $e^{iH_1 t/2} e^{iH_2 t/2}$ might approach the Haar measure much faster on a timescale independent of N [1, 5] (though dependent on k).

We extend this idea by further dividing t into n ranges, with each range evolving under a Hamiltonian H_n independently drawn from GUE, forming $U_t = e^{iH_1 t/n} e^{iH_2 t/n} \dots e^{iH_n t/n}$.

As $n \rightarrow \infty$, this approach effectively creates a Brownian model, which we refer to as the Brownian Gaussian Unitary Ensemble (BGUE).

In this paper, we explore BGUE in detail. We first investigate several exactly solvable results for its non-equilibrium dynamics at finite N and t . We then determine the time required for BGUE to approximate the Haar random ensemble, measured by k -design. Finally, we apply the BGUE model to classical shadow tomography, providing analytical results for the shadow norm and identifying an optimal time that minimizes it, akin to the optimal circuit depth in shallow-circuit shadow tomography schemes.

Model Considered We consider an $N \times N$ random Brownian Hamiltonian $H(t)$, where the matrix elements are zero-mean Gaussian random variables with the covariance:

$$\mathbb{E} [H_{ij}(t)H_{kl}(t')] = N^{-1}\delta_{il}\delta_{jk}\delta(t-t') \quad (1.1)$$

All higher-order correlators satisfy Wick's theorem. The evolution operator is defined as $U_t = \mathcal{P}_{\text{path}} \left[e^{i \int_0^t dt' H(t')} \right]$.

Summary of Results In section 2, we explore the non-equilibrium properties of BGUE. We calculate $\mathbb{E}[U_t \otimes U_t^*]$ and $\mathbb{E}[U_t \otimes U_t^* \otimes U_t \otimes U_t^*]$ exactly, providing explicit analytical expressions for various one-replica and two-replica variables as functions of arbitrary N and t . These variables include the spectral form factor (SFF) (2.17), two-point functions (2.18), fluctuations of SFF (2.19), fluctuations of two-point functions (2.21), out-of-time-order correlators (OTOC) (2.25), the second Rényi entropy (2.27), and the frame potential for unitary 2-designs (2.31).

Our findings reveal that BGUE exhibits hyperfast scrambling and the emergence of temperature [6]. We also discuss the replica-wormhole-like contribution in BGUE, leading to a non-decaying two-point function as $t \rightarrow +\infty$ [7, 8] and non-vanishing fluctuations of the two-point function with a zero mean value [9].

In section 3, we examine the complexity of BGUE, determining the time required for BGUE to approximate the Haar ensemble in terms of k -design [3, 4, 10–13]. In section 3.1, we study the low-energy eigen-wavefunctions, spectrum, and degeneracy of the effective imaginary-time evolution operator on $2k$ -replicated contours. Based on these results, in section 3.2, we obtain the frame potential $F_{\text{BGUE}}^{(k)}(t)$ for large but finite t (3.30) for arbitrary k , and the corresponding time (3.31) needed to approach a unitary k -design. This timescale is linear in $k \log N$, consistent with previous studies on the Brownian Sachdev-Ye-Kitaev (SYK) model [14–16]. In appendix A, we derive a subset of the high-energy spectrum.

In section 4, we apply BGUE to classical shadow tomography [17], obtaining analytical results for the shadow norm (4.12) and identifying an optimal time (4.13) when the observable O includes both diagonal and off-diagonal parts. This optimal time parallels the optimal circuit depth in shallow-circuit shadow tomography [18, 19].

Note Added. After completing this work, we noted the appearance of reference [20] on arXiv, which also studies the complexity of the BGUE model in their section 4. While we agree on results regarding the frame potential and k -design using different approaches, reference [20] focuses on the concept and formalism of complexity in more generic Brownian

models, including the Brownian Sachdev-Ye-Kitaev (SYK) model. Our work emphasizes on BGUE itself, examining many non-equilibrium properties and its applications in some quantum information tasks.

2 Non-equilibrium dynamics: exact results for one/two-replica variables

In this section, we investigate various aspects of the non-equilibrium dynamics of BGUE. For spectral properties, we study the Spectral Form Factor (SFF) and its fluctuation [21]. For correlation functions and scrambling behavior [15, 22, 23], we examine the two-point function and its fluctuation, as well as OTOC [15, 24–26]. Additionally, we study the second Rényi entropy of pure product states evolved under BGUE as a measure of entanglement generation [27–29].

These quantities depend on one or two replicas of $U_t \otimes U_t^*$; therefore, it is beneficial to first derive the averaged evolution operators on two/four contours: $\mathcal{U}_1(t) \equiv \mathbb{E}[U_t \otimes U_t^*]$ and $\mathcal{U}_2(t) \equiv \mathbb{E}[U_t \otimes U_t^* \otimes U_t \otimes U_t^*]$. This calculation scheme is similar to random tensor network models [30] and random unitary circuit models [27–29, 31, 32] extensively studied in previous literature concerning scrambling dynamics [27, 28], Measurement Induced Phase Transition (MIPT) [33–43], and the holographic theory of gravity [44–46]. A common feature of these models is that, due to the Brownian property, Hamiltonians (for continuous time evolution) or unitaries (for discrete time evolution) at different times are uncorrelated, meaning that the average taken at different times factorizes. For generic k -replica observables in BGUE, we ultimately obtain an imaginary time evolution on $2k$ -contours:

$$\mathcal{U}_k(t) \equiv \mathbb{E}[U_t^{\otimes k} \otimes U_t^{*\otimes k}] \equiv e^{\mathcal{L}_k t} \quad (2.1)$$

where \mathcal{L}_k is a Hermitian operator acting on $2k$ -contours. We make four further comments that might help readers better interpret equation (2.1):

1. *Time translation invariance of \mathcal{L}_k* : Although a single realization of BGUE lacks time translation invariance, it is restored after averaging.
2. *$\mathcal{U}_k(t)$ satisfies an ODE*: Namely $\partial_t \mathcal{U}_k(t) = \mathcal{L}_k \mathcal{U}_k(t)$. This is due to the Markovian property of Brownian models. For a static random Hamiltonian like GUE or SYK-model [15], we expect a more complicated differential-integral equation (the Schwinger-Dyson equation for SYK).
3. *$\mathcal{U}_k(t)$ is not unitary*: This is because a linear superposition of unitary matrices is generally not unitary.
4. *\mathcal{L}_k is Hermitian*: This follows from two reasons: the time-translation symmetry of the ensemble and the zero mean of $H(t)$, where the latter implies an additional symmetry $H(t) \rightarrow -H(t)$.

Prepared with this high-level outline of the calculation structure, we explicitly derive $\mathcal{L}_1, \mathcal{L}_2$ and $\mathcal{U}_1(t), \mathcal{U}_2(t)$ in section 2.1, and then apply these results to calculate observables in sections 2.2 and 2.3.

where we expand the exponential and drop the linear-in- Δt term since $H(t)$ has zero mean. We find that:

$$\mathcal{L}_k = -k + N^{-1} \sum_{i,\bar{j}=1}^k P_{i\bar{j}} - N^{-1} \sum_{1 \leq i < j \leq k} X_{ij} - N^{-1} \sum_{1 \leq \bar{i} < \bar{j} \leq k} X_{\bar{i}\bar{j}} \quad (2.6)$$

Exponentiating \mathcal{L}_k to obtain $\mathcal{U}_k(t) = e^{\mathcal{L}_k t}$ is challenging for generic k . This is because $\{P_{i\bar{j}}, X_{ij}, X_{\bar{i}\bar{j}}\}$ are the generators of a non-trivial algebra, which is a sub-algebra of the partition algebra [47]. Therefore, the task of exponentiating \mathcal{L}_k is equivalent to finding the corresponding representation of this algebra.

Fortunately, for the special case of $k = 1, 2$, we can calculate $\mathcal{U}_k(t)$ exactly, using the idea of Krylov space described below.

Two-contour averaged evolution operator. According to equation (2.6), \mathcal{L}_1 is very simple:

$$\mathcal{L}_1 = -1 + N^{-1} P_{1\bar{1}} \quad (2.7)$$

Using the property $P_{i\bar{j}}^2 = N P_{i\bar{j}}$, we obtain:

$$\mathcal{U}_1(t) = e^{-t} \mathbb{I} + (1 - e^{-t}) N^{-1} P_{1\bar{1}} \quad (2.8)$$

A quick consistency check is to calculate $\text{tr}[U_t U_t^\dagger] = N$ using $\mathcal{U}_1(t)$, which is realized by $\langle \text{EPR}_{1\bar{1}} | \mathcal{U}_1 | \text{EPR}_{1\bar{1}} \rangle = e^{-t} N + (1 - e^{-t}) N = N$.

We also notice that when $t \rightarrow +\infty$, $\mathcal{U}_1(+\infty) = N^{-1} P_{1\bar{1}}$ matches the expectation from the Haar random ensemble. This suggests that our BGUE smoothly interpolates between the identity unitary and the Haar ensemble through time evolution. We will see more evidence of this in higher replicas.

Four-contour averaged evolution operator. Similarly, using equation (2.6), we obtain \mathcal{L}_2 :

$$\mathcal{L}_2 = -2 + N^{-1} (P_{1\bar{1}} + P_{2\bar{2}} + P_{1\bar{2}} + P_{2\bar{1}}) - N^{-1} (X_{12} + X_{\bar{1}\bar{2}}) \quad (2.9)$$

where X_{12} is the SWAP operator between 1 and 2.

Next, we need to exponentiate \mathcal{L}_2 , which is more complicated than exponentiating \mathcal{L}_1 . The trick is to notice that the Krylov space [48–55] of \mathcal{L}_2 , defined as polynomials of \mathcal{L}_2 , $\mathcal{K} \equiv \text{span}\{1, \mathcal{L}_2, \mathcal{L}_2^2, \mathcal{L}_2^3, \dots\}$, is finite-dimensional. This is because the product of links are still links, and there are a total of $4! = 24$ types of links, corresponding to the 24 permutation elements of \mathbb{S}^4 . Further dimension reduction can be made by noting the symmetry of \mathcal{L}_2 : permutation of four contours and Hermiticity. We group all 24 link operators into 8 categories, serving as the basis of the Krylov space, namely $\mathcal{K} = \text{span}\{A_i | i = 1, \dots, 8\}$:

$$\begin{aligned}
A_1 &= \begin{array}{c} \text{---} \\ \text{---} \\ \text{---} \\ \text{---} \end{array} \begin{array}{c} 1 \\ \bar{1} \\ 2 \\ \bar{2} \end{array} = 1 \\
A_2 &= \begin{array}{c} \text{)} \\ \text{---} \\ \text{---} \end{array} \begin{array}{c} \text{C} \\ \text{---} \\ \text{---} \end{array} + \begin{array}{c} \text{---} \\ \text{---} \\ \text{---} \end{array} \begin{array}{c} \text{---} \\ \text{---} \\ \text{---} \end{array} + \begin{array}{c} \text{---} \\ \text{---} \\ \text{---} \end{array} \begin{array}{c} \text{---} \\ \text{---} \\ \text{---} \end{array} = P_{1\bar{1}} + P_{2\bar{2}} + P_{1\bar{2}} + P_{2\bar{1}} \\
A_3 &= \begin{array}{c} \text{---} \\ \text{---} \\ \text{---} \end{array} + \begin{array}{c} \text{---} \\ \text{---} \\ \text{---} \end{array} = X_{12} + X_{\bar{1}\bar{2}} \\
A_4 &= \begin{array}{c} \text{)} \\ \text{---} \\ \text{---} \end{array} \begin{array}{c} \text{C} \\ \text{---} \\ \text{---} \end{array} + \begin{array}{c} \text{)} \\ \text{---} \\ \text{---} \end{array} \begin{array}{c} \text{C} \\ \text{---} \\ \text{---} \end{array} + \begin{array}{c} \text{)} \\ \text{---} \\ \text{---} \end{array} \begin{array}{c} \text{C} \\ \text{---} \\ \text{---} \end{array} + \begin{array}{c} \text{)} \\ \text{---} \\ \text{---} \end{array} \begin{array}{c} \text{C} \\ \text{---} \\ \text{---} \end{array} + \begin{array}{c} \text{)} \\ \text{---} \\ \text{---} \end{array} \begin{array}{c} \text{C} \\ \text{---} \\ \text{---} \end{array} + \begin{array}{c} \text{)} \\ \text{---} \\ \text{---} \end{array} \begin{array}{c} \text{C} \\ \text{---} \\ \text{---} \end{array} + \begin{array}{c} \text{)} \\ \text{---} \\ \text{---} \end{array} \begin{array}{c} \text{C} \\ \text{---} \\ \text{---} \end{array} \quad (2.10) \\
A_5 &= \begin{array}{c} \text{)} \\ \text{---} \\ \text{---} \end{array} \begin{array}{c} \text{C} \\ \text{---} \\ \text{---} \end{array} + \begin{array}{c} \text{)} \\ \text{---} \\ \text{---} \end{array} \begin{array}{c} \text{C} \\ \text{---} \\ \text{---} \end{array} \\
A_6 &= \begin{array}{c} \text{---} \\ \text{---} \\ \text{---} \end{array} \\
A_7 &= \begin{array}{c} \text{)} \\ \text{---} \\ \text{---} \end{array} \begin{array}{c} \text{C} \\ \text{---} \\ \text{---} \end{array} + \begin{array}{c} \text{)} \\ \text{---} \\ \text{---} \end{array} \begin{array}{c} \text{C} \\ \text{---} \\ \text{---} \end{array} \\
A_8 &= \begin{array}{c} \text{)} \\ \text{---} \\ \text{---} \end{array} \begin{array}{c} \text{C} \\ \text{---} \\ \text{---} \end{array} + \begin{array}{c} \text{)} \\ \text{---} \\ \text{---} \end{array} \begin{array}{c} \text{C} \\ \text{---} \\ \text{---} \end{array} + \begin{array}{c} \text{)} \\ \text{---} \\ \text{---} \end{array} \begin{array}{c} \text{C} \\ \text{---} \\ \text{---} \end{array} + \begin{array}{c} \text{)} \\ \text{---} \\ \text{---} \end{array} \begin{array}{c} \text{C} \\ \text{---} \\ \text{---} \end{array}
\end{aligned}$$

In these diagrams, the contours are arranged in the order $1, \bar{1}, 2, \bar{2}$ from top to bottom (see diagram of A_1 in (2.10)). We note that $\mathcal{L}_2 = -2A_1 + N^{-1}A_2 - N^{-1}A_3 \equiv \sum_i v_i^{(1)} A_i$. We also define $\mathcal{L}_2^n = \sum_i v_i^{(n)} A_i$. We can work out the matrix representation of \mathcal{L}_2 on this basis. Define $\mathcal{L}_2 A_i = \sum_j M_{ji} A_j$, the 8×8 representation matrix M is explicitly given by:

$$M = \begin{pmatrix} -2 & 0 & -2N^{-1} & 0 & 0 & 0 & 0 & 0 \\ N^{-1} & -1 & 0 & 0 & 0 & 0 & 0 & 0 \\ -N^{-1} & 0 & -2 & 0 & 0 & -N^{-1} & 0 & 0 \\ 0 & 0 & N^{-1} & -1 & 0 & 0 & 0 & 0 \\ 0 & 2N^{-1} & 0 & 0 & 0 & 0 & 0 & 2N^{-1} \\ 0 & 0 & -2N^{-1} & 0 & 0 & -2 & 0 & 0 \\ 0 & 0 & 0 & 4N^{-1} & 0 & 0 & 0 & 0 \\ 0 & 0 & 0 & 0 & 0 & N^{-1} & 0 & -1 \end{pmatrix} \quad (2.11)$$

From the form of M , we immediately observe the following:

1. *Steady correlation patterns:* $\mathcal{L}_2 A_5 = \mathcal{L}_2 A_7 = 0$, meaning that these two bases are stationary. They directly correspond to the correlation patterns of the Haar ensemble [56–60], which persist in the $t \rightarrow \infty$ limit.
2. *Transient correlation patterns:* The off-diagonal entries of M are suppressed by large N , so for large N , only the diagonal entries (contributed solely from $(P_{1\bar{1}} + P_{2\bar{2}} + P_{1\bar{2}} + P_{2\bar{1}})$, with $N^{-1}(X_{12} + X_{\bar{1}\bar{2}})$ only contributing to off-diagonals) are significant, which are of order one. Therefore, the diagonals are all negative for $A_i, i \in \{1, 2, 3, 4, 6, 8\}$,

indicating that these correlation patterns eventually fade away. This holds for general k . The correlation patterns connecting the left ($t = t_{\text{final}}$) and right boundary ($t = 0$) will fade away, leaving only left/left or right/right patterns, which sum up to be the projectors of the Haar ensemble. This conjecture for general k will be further clarified in section 3.1.

3. *Pseudo-Hermiticity*: \mathcal{L}_2 is a Hermitian operator, but its representation matrix M is non-Hermitian. This is because the basis $\{A_i\}$ is not orthogonal, making M pseudo-Hermitian.

Knowing the 8×8 matrix M and the 8×1 column vector $v^{(1)}$, we have:

$$e^{\mathcal{L}_2 t} = A_1 + \sum_{i=1}^8 \left[(e^{Mt} - 1) M^{-1} v^{(1)} \right]_i A_i \quad (2.12)$$

where M^{-1} is interpreted as the pseudo-inverse of M , since M itself is not invertible due to two zero modes.

It is instructive to study the spectrum of M . The eight eigenvalues λ_i are given by:

$$\lambda_i = 0, 0, -1, -1, -1, -(2 - 2N^{-1}), -2, -(2 + 2N^{-1}) \quad (2.13)$$

We see that the $0, -1, -2$ eigenvalues are expected since the four-contour evolution is schematically the square of two-contour evolution, where the latter has $\{1, e^{-t}\}$ modes, so its square naturally includes $\{1, e^{-t}, e^{-2t}\}$ modes. The new modes are $\lambda_i = -2 \pm 2N^{-1}$, which have non-trivial N -dependence. This effect is non-perturbative.

Denoting V as the eigenvector matrix of M (each column of V is a left-eigenvector of M , which does not need to be orthogonal) and D as the diagonal matrix of eigenvalues of M , we can easily exponentiate M , and the final result is:

$$\mathcal{U}_2(t) = e^{\mathcal{L}_2 t} = \sum_{i=1}^8 \left[\delta_{i1} + V(e^{Dt} - 1)V^{-1}M^{-1}v^{(1)} \right]_i A_i \equiv \sum_{i=1}^8 f_i(t) A_i \quad (2.14)$$

The time-dependent coefficients $f_i(t)$ in front of each correlation pattern are given explicitly by:

$$\begin{pmatrix} f_1(t) \\ f_2(t) \\ f_3(t) \\ f_4(t) \\ f_5(t) \\ f_6(t) \\ f_7(t) \\ f_8(t) \end{pmatrix} = \begin{pmatrix} 0 & 0 & \frac{1}{4} & \frac{1}{2} & \frac{1}{4} \\ 0 & \frac{N^2-2}{N(N^2-4)} & \frac{-1}{4(N-2)} & \frac{-1}{2N} & \frac{-1}{4(N+2)} \\ 0 & 0 & -\frac{1}{4} & 0 & \frac{1}{4} \\ 0 & \frac{-1}{N^2-4} & \frac{1}{4(N-2)} & 0 & \frac{-1}{4(N+2)} \\ \frac{1}{N^2-1} & \frac{-2}{N^2-4} & \frac{1}{2(N-1)(N-2)} & 0 & \frac{1}{2(N+1)(N+2)} \\ 0 & 0 & \frac{1}{4} & -\frac{1}{2} & \frac{1}{4} \\ \frac{-1}{N^3-N} & \frac{4}{N(N^2-4)} & \frac{-1}{2(N-1)(N-2)} & 0 & \frac{1}{2(N+1)(N+2)} \\ 0 & \frac{2}{N(N^2-4)} & \frac{-1}{4(N-2)} & \frac{1}{2N} & \frac{-1}{4(N+2)} \end{pmatrix} \times \begin{pmatrix} 1 \\ e^{-t} \\ e^{-(2-2N^{-1})t} \\ e^{-2t} \\ e^{-(2+2N^{-1})t} \end{pmatrix} \quad (2.15)$$

where we express it in a compact way by decomposing it into five distinct modes.

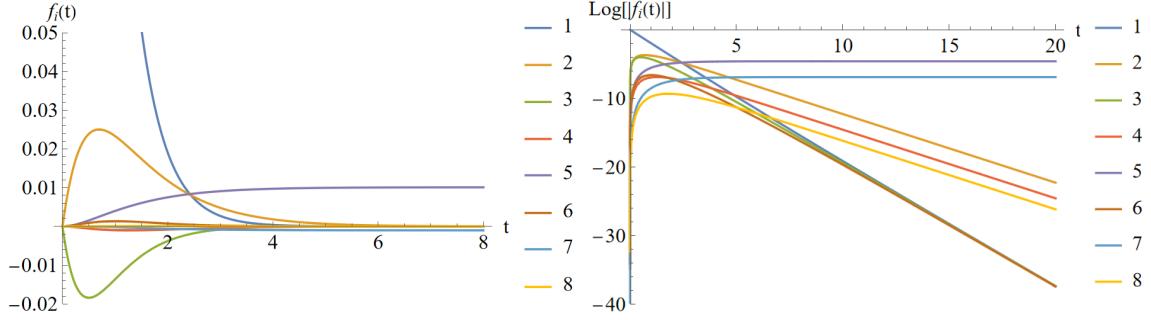


Figure 1. The pattern coefficient $f_i(t)$ or its log-plot, evaluated at $N = 10$ according to equation (2.15). From the log-plot, we can easily see the exponentially decaying modes, and $f_5(t), f_7(t)$ remain finite at $t = +\infty$.

We can perform some explicit sanity checks: (1) the first column of the coefficient matrix in (2.15) shows that only f_5, f_7 are non-zero at $t = +\infty$. The two non-zero entries of first column, $\frac{1}{N^2-1}$ and $\frac{-1}{N^3-N}$, coincide with the correct Weingarten functions of the Haar ensemble; (2) one can check that the normalization is correct by noting that we should have $\text{tr}[U_t U_t^\dagger] \text{tr}[U_t U_t^\dagger] = N^2$, which is realized by $\langle \text{EPR}_{1\bar{1}} \text{EPR}_{2\bar{2}} | \mathcal{U}_4 | \text{EPR}_{1\bar{1}} \text{EPR}_{2\bar{2}} \rangle = \sum_i f_i(t) \text{tr}[A_i]$; (3) At $t = 0$, only $f_1 = 1$ and other coefficients are zero.

In figure 1, we plot the correlation pattern coefficient $f_i(t)$ as a function of time. We see that some transient correlation patterns that connect the left-boundary condition and right-boundary condition may appear at intermediate times. However, they eventually die out at long real-time, leaving only A_5 and A_7 :

$$\mathcal{U}_2(+\infty) = f_5(+\infty)A_5 + f_7(+\infty)A_7 = \int_{\text{Haar}} dU \cdot U \otimes U^* \otimes U \otimes U^* \quad (2.16)$$

This means that $\mathcal{U}_2(+\infty)$ equals the prediction of the Haar ensemble [56–60]. In section 3.1, we will show that $\mathcal{U}_k(t = +\infty)$ equals the Haar’s prediction for arbitrary k .

We are now ready to apply the result of $\mathcal{U}_1(t)$ in (2.8) and the result of $\mathcal{U}_2(t)$ in (2.14), (2.10), and (2.15) to calculate observables.

2.2 One-replica observables

Spectral Form Factor. The spectral form factor (SFF) is given by:

$$\mathbb{E}[\text{SFF}(t)] \equiv \mathbb{E} \left[\text{tr}(U_t) \text{tr}(U_t^\dagger) \right] = N^2 e^{-t} + (1 - e^{-t}) \quad (2.17)$$

which smoothly interpolates between the identity and Haar ensemble. We see that at the timescale $t \sim O(\log N^2)$, the two terms become comparable, and SFF is of order one.

Similar to the Brownian SYK, SFF in BGUE monotonically decreases with time, and there is no linear ramp as in the static GUE or static SYK model [21]. In figure 2, we plot SFF with respect to time.

Two-point function. Consider the following two-point function:

$$\mathbb{E}[C(t)] \equiv \mathbb{E}[\text{tr}(AB_t)] = \mathbb{E}[\text{tr}(AU_t B U_t^\dagger)] = \text{tr}(AB) e^{-t} + N^{-1} \text{tr}(A) \text{tr}(B) (1 - e^{-t}) \quad (2.18)$$

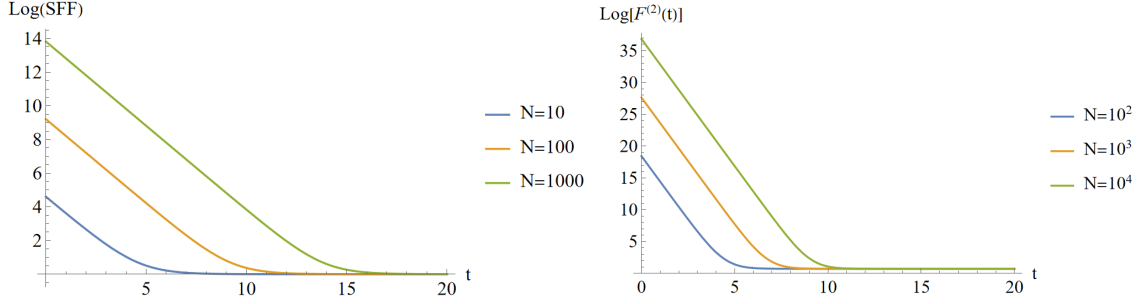


Figure 2. **Left:** Log of the average value of the spectral form factor (2.17) with respect to time. **Right:** Log of the frame potential (2.31) with respect to time.

which smoothly interpolates between $\text{tr}(AB)$ and $\text{tr}(A)\text{tr}(B)$. This indicates that the correlation connecting the left and right of the contour gradually dies out at the timescale $t \sim O(1)$.

It is helpful to compare this with the result of BDSSYK (Brownian Double-Scaled-SYK), whose two-point function has the form of $e^{-\frac{J^2}{\lambda}(1-q_V)t}$ [44, 45]. There are several immediate remarks:

1. *Emergence of temperature in BGUE.* The emergence of a timescale in infinite temperature (Brownian has no energy conservation) is like temperature [6].
2. *Replica-wormhole in BGUE.* There is no replica wormhole in BDSSYK. This is because we already take the infinite dimension limit, and all higher topological changes are suppressed. In our BGUE model, the non-decaying part of the two-point function [7–9] $\mathbb{E}[C(t = +\infty)] = N^{-1} \text{tr}(A)\text{tr}(B)$ is reminiscent of the replica wormhole [61, 62].
3. *Dependence on matter scaling dimension.* In BDSSYK, the scaling dimension of matter chords, q_V , appears in the exponent, which affects the timescale explicitly. In BGUE, the matter operators only appear as the boundary condition, and the damping mode only depends on \mathcal{L}_2 . BGUE is recovered as a special limit in BDSSYK by taking the q -parameter to zero.

2.3 Two-replica observables

Fluctuation of spectral form factor.

$$\begin{aligned} \text{Var}[\text{SFF}(t)] &\equiv \mathbb{E}[\text{tr}(U_t)\text{tr}(U_t^\dagger)\text{tr}(U_t)\text{tr}(U_t^\dagger)] - \mathbb{E}[\text{tr}(U_t)\text{tr}(U_t^\dagger)]\mathbb{E}[\text{tr}(U_t)\text{tr}(U_t^\dagger)] \\ &= 1 + 2(N^2 - 1)e^{-t} + N^2e^{-2t} \left(N^2 \sinh^2 \frac{t}{N} - N \sinh \frac{t}{N} - \frac{3}{2} \cosh \frac{2t}{N} - \frac{1}{2} + N^{-2} \right) \end{aligned} \quad (2.19)$$

We notice that $\text{Var}[\text{SFF}(0)] = 0$, which is reasonable, and $\text{Var}[\text{SFF}(+\infty)] = 1$. We can also fix t and scale N to infinity:

$$\lim_{N \rightarrow \infty} \text{Var}[\text{SFF}(t)] = N^2 [2e^{-t} + e^{-2t}(t^2 - t - 2)] \quad (2.20)$$

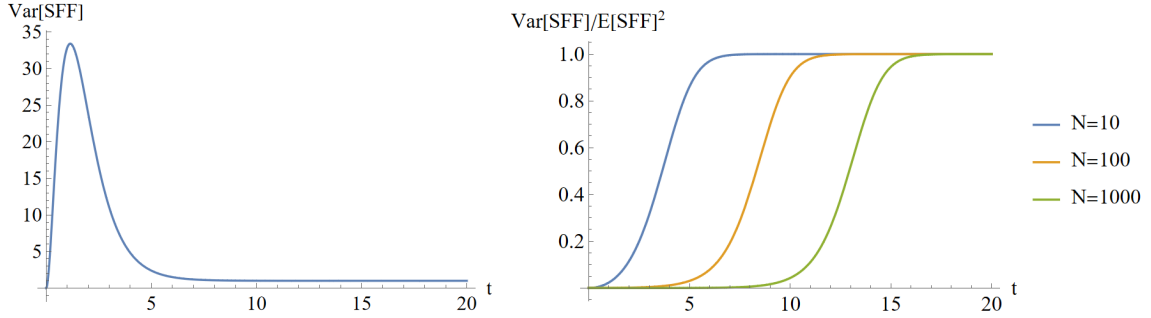


Figure 3. Left: The absolute variance of the spectral form factor (2.19), dimension chosen at $N = 10$. **Right:** The relative variance of SFF.

Therefore, the maximal value of variance is of order $O(N^2)$, and the timescale for reaching this maximal fluctuation is of order one.

A more physical way of quantifying the size of the fluctuation is to calculate the relative variance: $\eta(t) \equiv \text{Var}[\text{SFF}(t)] / \mathbb{E}[\text{SFF}(t)]^2$, which is shown in figure 3. We see that for $t < O(\log N^2)$, $\eta \approx 0$, and for $t > O(\log N^2)$, $\eta \approx 1$. This is consistent with the case in GUE or SYK, where the fluctuation in the plateau regime is large compared to the dip regime [21].

Fluctuation of two-point functions. In general, the expression for the fluctuation of the two-point function is complicated, as calculating $\mathbb{E}[\text{tr}(AB_t) \text{tr}(AB_t)]$ involves many contour pairings, where each of the A_i terms will contribute respectively as: $A_1 \rightarrow \text{tr}[AB]^2$, $A_2 \rightarrow 2 \text{tr}[AB] \text{tr}[A] \text{tr}[B] + 2 \text{tr}[A^2 B^2]$, $A_3 \rightarrow 2 \text{tr}[ABAB]$, $A_4 \rightarrow 4 \text{tr}[B] \text{tr}[BA^2] + 4 \text{tr}[A] \text{tr}[AB^2]$, $A_5 \rightarrow \text{tr}[A]^2 \text{tr}[B]^2 + \text{tr}[A^2] \text{tr}[B^2]$, $A_6 \rightarrow \text{tr}[AB]^2$, $A_7 \rightarrow \text{tr}[A]^2 \text{tr}[B^2] + \text{tr}[B]^2 \text{tr}[A^2]$, $A_8 \rightarrow 2 \text{tr}[A] \text{tr}[B] \text{tr}[AB] + 2 \text{tr}[A^2 B^2]$. To simplify the expression, we consider three cases:

1. *Case 1:* $\text{tr}[A] = \text{tr}[B] = \text{tr}[AB] = 0$, $A^2 = B^2 = 1$, $AB = BA$, where we imagine A, B are Pauli operators on different spatial sites. In this case, we have $\mathbb{E}[C_1(t)] = 0$, meaning the average two-point function vanishes.
2. *Case 2:* $\text{tr}[A] = \text{tr}[B] = \text{tr}[AB] = 0$, $A^2 = B^2 = 1$, $AB = -BA$, where we imagine A, B are Pauli operators on the same spatial site, but with different flavors. In this case, we have $\mathbb{E}[C_2(t)] = 0$, meaning the average two-point function vanishes.
3. *Case 3:* $A = B$, $\text{tr}[A] = 0$, $A^2 = 1$, where we consider the auto-correlation of a Pauli operator. In this case, we have $\mathbb{E}[C_3(t)] = N e^{-t}$.

The variance of these three types of correlation functions is given by:

$$\begin{aligned}
 \text{Var}[C_1(t)] &= \frac{N^2}{N^2 - 1} - \frac{N^2}{2(N - 1)} e^{-(2-2N^{-1})t} + \frac{N^2}{2(N + 1)} e^{-(2+2N^{-1})t} \\
 \text{Var}[C_2(t)] &= \frac{N^2}{N^2 - 1} + \frac{N(N - 2)}{2(N - 1)} e^{-(2-2N^{-1})t} - \frac{N^2}{N(N + 2)} e^{-(2+2N^{-1})t} \\
 \text{Var}[C_3(t)] &= \frac{N^2}{N^2 - 1} + \frac{N^2(N - 2)}{2(N - 1)} e^{-(2-2N^{-1})t} - N^2 e^{-2t} + \frac{N^2(N + 2)}{2(N + 1)} e^{-(2+2N^{-1})t}
 \end{aligned} \tag{2.21}$$

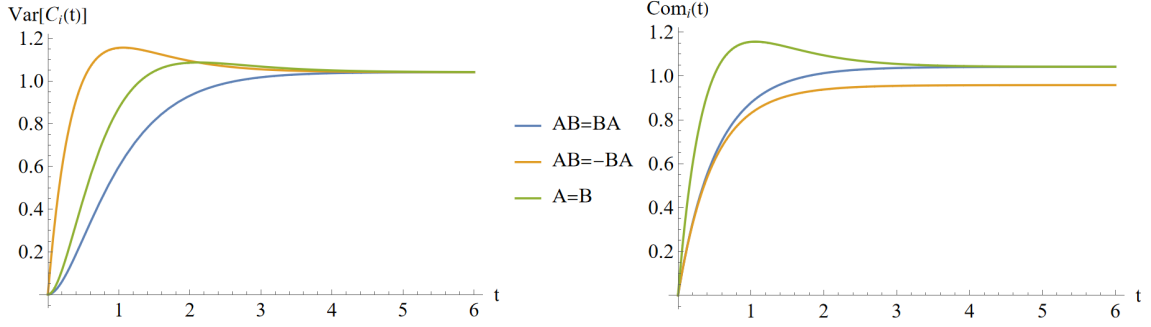


Figure 4. Left: Fluctuation of two-point functions (2.21). **Right:** Average value of commutator squared (2.25). In both figures, the dimension is chosen at $N = 5$.

We notice that the variance is of order one at arbitrary t, N . This finite variance is non-trivial for $C_1(t)$ and $C_2(t)$, since their average values vanish. This non-zero variance with zero mean is due to the effect of the replica wormhole, as indicated in [9].

These three fluctuations are shown in figure 4, where we see that at intermediate times, the behavior of fluctuation depends on whether A, B commute or anti-commute, and also on whether A, B are the same or not. This originates from terms like $\text{tr}[ABAB], \text{tr}[AB]$, whose coefficients are non-zero only at intermediate times.

We also notice that the initial growth of variance differs in the three cases. To see this, we may work out the Taylor expansion at short times:

$$\begin{aligned}
 \text{Var}[C_1(t)] &= 2t^2 - \frac{8}{3}t^3 + \frac{2(3N^2 + 1)}{3N^2}t^4 + O(t^5) \\
 \text{Var}[C_2(t)] &= 4t - 6t^2 + \frac{8(2N^2 + 1)}{3N^2}t^3 + O(t^4) \\
 \text{Var}[C_3(t)] &= 4t^2 - \frac{20}{3}t^3 + \frac{2(9N^2 + 1)}{3N^2}t^4 + O(t^5)
 \end{aligned} \tag{2.22}$$

It is interesting to see that for C_2 , the variance grows linearly while the others grow quadratically. It is also interesting to observe that the first two coefficients are independent of N .

We can also work out the limit where N goes to infinity while keeping t fixed, where the variance is of order one:

$$\begin{aligned}
 \lim_{N \rightarrow \infty} \text{Var}[C_1(t)] &= 1 + e^{-2t}(-2t - 1) \\
 \lim_{N \rightarrow \infty} \text{Var}[C_2(t)] &= 1 + e^{-2t}(2t - 1) \\
 \lim_{N \rightarrow \infty} \text{Var}[C_3(t)] &= 1 + e^{-2t}(2t^2 - 2t - 1)
 \end{aligned} \tag{2.23}$$

Out-of-Time-Ordered Correlator (OTOC) Assuming $A^2 = B^2 = 1$, the relation between (anti)commutator-squared and OTOC is given by:

$$\text{Com}(t) \equiv (2N)^{-1} \text{tr} \left([A, B_t]_{\pm}^{\dagger} [A, B_t]_{\pm} \right) = 1 \pm N^{-1} \text{tr} (AB_t AB_t) = 1 \pm \text{OTOC}(t) \tag{2.24}$$

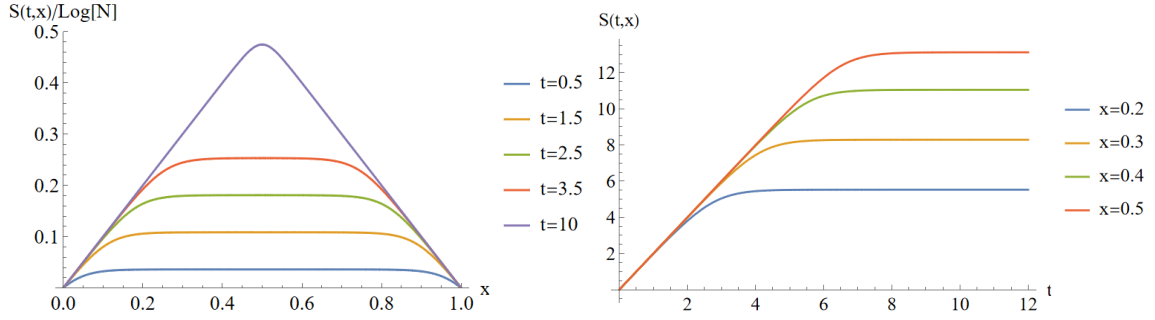


Figure 5. The entanglement entropy (2.27) changes with respect to subsystem size and time. Size is taken to be $N = 10^{12}$.

where we choose (anti)commutator and (plus)minus sign on RHS if at the initial time A, B (anti)commute with each other. The commutator of three cases is given by:

$$\begin{aligned}
\mathbb{E}[\text{Com}_1(t)] &= 1 + \frac{1}{N^2 - 1} - \frac{N}{2(N-1)}e^{-(2-2N^{-1})t} - \frac{N}{2(N+1)}e^{-(2+2N^{-1})t} \\
\mathbb{E}[\text{Com}_2(t)] &= 1 - \frac{1}{N^2 - 1} - \frac{N-2}{2(N-1)}e^{-(2-2N^{-1})t} - \frac{N+2}{2(N+1)}e^{-(2+2N^{-1})t} \\
\mathbb{E}[\text{Com}_3(t)] &= 1 + \frac{1}{N^2 - 1} + \frac{N(N-2)}{2(N-1)}e^{-(2-2N^{-1})t} - \frac{N(N+2)}{2(N+1)}e^{-(2+2N^{-1})t}
\end{aligned} \tag{2.25}$$

We may take $N \rightarrow \infty$ while keeping t finite:

$$\begin{aligned}
\lim_{N \rightarrow \infty} \mathbb{E}[\text{Com}_1(t)] &= 1 - e^{-2t} \\
\lim_{N \rightarrow \infty} \mathbb{E}[\text{Com}_2(t)] &= 1 - e^{-2t} \\
\lim_{N \rightarrow \infty} \mathbb{E}[\text{Com}_3(t)] &= 1 + e^{-2t}(2t - 1)
\end{aligned} \tag{2.26}$$

We note that OTOC and commutators still have non-trivial dynamics in the infinite N limit. This hyper-fast scrambling behavior [6, 63–70] is consistent with other Brownian models such as BDSSYK [44, 45]. This is opposed to static SYK, where the timescale for scrambling is $O(\log N)$ [15], meaning no scrambling dynamics will occur at infinite N . The behavior of commutators is shown in figure 4.

Second Rényi Entropy Consider we evolve the system from a pure product state. At time t , we consider the sub-system with Hilbert space dimension N^x , $x \in [0, 1]$. The second Rényi entropy (actually we first average over the purity, and then take the log) is given by:

$$S^{(2)}(t, x) = -\log \left[e^{-(2+2N^{-1})t} + \frac{N^x + N^{1-x}}{N+1} \left(1 - e^{-(2+2N^{-1})t} \right) \right] \tag{2.27}$$

We see that the system approaches the Page curve of the Haar random ensemble at order one time, consistent with studies in the scrambling phase of MIPT in (0+1)-dimensional models [33–43].

We can also study the velocity of entropy growth at the initial time:

$$S^{(2)}(t, x) = 2(1 - N^{-x})(1 - N^{-(1-x)})t - 2(1 - N^{-x})(1 - N^{-(1-x)})(N^{-x} + N^{-(1-x)})t^2 + O(t^3) \quad (2.28)$$

We see that the coefficient of t approaches 2 for arbitrary x in the infinite N limit, and the coefficient of t^2 vanishes in the infinite N limit. This shows that in the infinite N limit, the linear-in-time growth rate of entropy for all subsystems is the same:

$$\lim_{N \rightarrow \infty} S^{(2)}(t, x) = 2t, \quad t < O(\log N) \quad (2.29)$$

Such a growth rate can be interpreted from (2.27). We notice that for $x \neq 0, x \neq 1$ and small t before saturation, the second term $\frac{N^x + N^{1-x}}{1+N}$ is of order $O(N^{-\min(x, 1-x)}) \ll O(1)$, which is always subleading in the infinite N limit compared to the first term. Therefore, we can safely approximate $S^{(2)}(t, x) \approx -\log[e^{-(2+2N^{-1})t}] = 2(1 + N^{-1})t \approx 2t$. The entropy curve is shown in figure 5.

Frame potential for unitary two-design Given any ensemble \mathcal{E} of unitary matrices, the frame potential [3, 4, 12, 16, 71–73], relevant to k -designs, is defined as:

$$F_{\mathcal{E}}^{(k)}(t) = \mathbb{E}_{U, V \in \mathcal{E}} \left[\left| \text{tr}(UV^\dagger) \right|^{2k} \right] \quad (2.30)$$

where U and V are drawn independently from the same ensemble \mathcal{E} .

Frame potential naturally measures whether \mathcal{E} is 'dispersed' or 'concentrated'. Consider an extreme case where the ensemble consists of only one element with probability one. In this case, the forward evolution perfectly cancels the backward evolution, leading to $\text{tr}(UV^\dagger) = \text{tr}(\mathbb{I}) = N$, which results in the maximal possible value of the frame potential. On the other hand, if \mathcal{E} is dispersed, then two independently drawn samples U and V are likely to be very different, meaning that $\text{tr}(UV^\dagger)$ will be very small. The most 'dispersed' ensemble is the Haar ensemble, indicating that $F_{\text{Haar}}^{(k)}$ is the smallest among all \mathcal{E} .

In our case, we can calculate $k = 2$, which is relevant for comparing 2-designs. For the identity ensemble (an ensemble whose single element is the identity matrix), $F_{\text{id}}^{(2)} = N^4$ and for the Haar random ensemble we have $F_{\text{Haar}}^{(2)} = 2! = 2$.

The formula for the frame potential of BGUE is $F_{\text{BGUE}}^{(2)}(t) = \text{tr}[e^{\mathcal{L}2t} \times e^{\mathcal{L}2t}] = \text{tr}[e^{\mathcal{L}22t}] = \mathbb{E}[\text{SFF}(2t)\text{SFF}(2t)]$, which is the square of the average spectral form factor. The explicit formula is given by:

$$F_{\text{BGUE}}^{(2)}(t) = 2 + 4(N^2 - 1)e^{-2t} + \frac{1}{4}N^2(N + 1)(N - 3)e^{-(4-4N^{-1})t} + \frac{1}{2}(N^2 - 1)(N^2 - 4)e^{-4t} + \frac{1}{4}N^2(N - 1)(N + 3)e^{-(4+4N^{-1})t} \quad (2.31)$$

which smoothly interpolate between $F_{\text{id}}^{(2)}$ and $F_{\text{Haar}}^{(2)}$. In section 3.2, we obtain the frame potential for arbitrary k up to the second excited states of \mathcal{L}_k . For $k = 2$, the second excited states are already the highest energy states.

3 Approaching k -design for arbitrarily many replicas

In this section, we are interested in how $\mathcal{U}_k(t)$ approaches the Haar ensemble's prediction for large but finite t . Therefore, in section 3.1, we focus on the low-energy spectrum (up to the family of second excited states) of $-\mathcal{L}_k$, which governs the long-time behavior of $\mathcal{U}_k(t)$. Using this spectral information, in section 3.2, we calculate the frame potential $F^{(k)}(t)$ and estimate a lower bound on the time needed to approach an ε -approximated k -design.

Recall there are k -replicas with k forward-moving contours labeled by $i = 1, 2, \dots, k$ and k backward-moving contours labeled by $\bar{i} = 1, 2, \dots, k$. The Hilbert space is $(\mathbb{C}^{\otimes N})^{\otimes 2k}$. The averaged evolution operator is defined by:

$$\mathcal{U}_k(t) = \mathbb{E} \left[U_t^{\otimes k} \otimes U_t^{*\otimes k} \right] = e^{\mathcal{L}_k t} \quad (3.1)$$

The Lindbladian is given by:

$$\begin{aligned} \mathcal{L}_k &= -k + N^{-1} \sum_{i, \bar{j}=1}^k P_{i\bar{j}} - N^{-1} \sum_{1 \leq i < j \leq k} X_{ij} - N^{-1} \sum_{1 \leq \bar{i} < \bar{j} \leq k} X_{\bar{i}\bar{j}} \\ &\equiv -k + N^{-1} \mathcal{P} - N^{-1} \mathcal{X} - N^{-1} \bar{\mathcal{X}} \end{aligned} \quad (3.2)$$

3.1 Low energy spectrum

3.1.1 Ground states

In this section, we show that the ground state energy of \mathcal{L}_k is zero, with degeneracy $k!$. The ground state manifold is spanned by permutation matrix elements. The projector onto the ground state manifold equals the prediction of the Haar average, indicating that $\mathcal{U}_k(t)$ approaches the Haar ensemble as $t \rightarrow +\infty$.

To be precise, the ground state of \mathcal{L}_k is labeled by a permutation element $\pi \in \mathbb{S}^k$:

$$|\pi\rangle : \langle n_1 \dots n_i \dots n_k, n_{\bar{1}} \dots n_{\bar{i}} \dots n_{\bar{k}} | \pi \rangle = \delta_{n_1 n_{\pi(1)}} \cdots \delta_{n_i n_{\pi(i)}} \cdots \delta_{n_k n_{\pi(k)}} \quad (3.3)$$

where $n_i, n_{\bar{i}} = 1, 2, \dots, N$ is the basis label on the individual Hilbert space of each contour. A diagrammatic example for $k = 4$ is:

$$|\pi\rangle = \begin{array}{c} 1 \\ 2 \\ 3 \\ 4 \\ \bar{1} \\ \bar{2} \\ \bar{3} \\ \bar{4} \end{array} \begin{array}{c} \text{---} \\ \text{---} \\ \text{---} \\ \text{---} \\ \text{---} \\ \text{---} \\ \text{---} \\ \text{---} \end{array} \text{ , } \pi \in \mathbb{S}^4 \quad (3.4)$$

In these diagrams, the $2k$ -contours are arranged from up to down in the order of $1, 2, \dots, k, \bar{1}, \bar{2}, \dots, \bar{k}$ (see the label in (3.4) for example). Notice that in section 2, the diagram for equation (2.10) for $k = 2$, the contour is ordered as $1, \bar{1}, 2, \bar{2}$ from up to down.

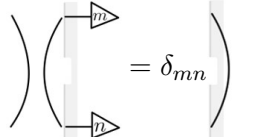
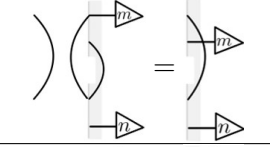
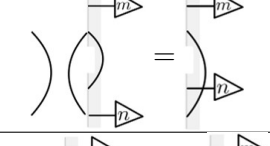
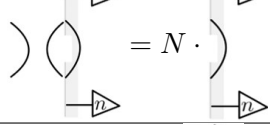
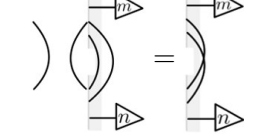
Label	Equation	#
1		1
2		$k - 1$
3		$k - 1$
4		$k - 1$
5		$2 \binom{k-1}{2}$

Table 1. $\mathcal{P}|mn, i\bar{j}, \pi\rangle$ is grouped into five categories. Notice that the total number of terms is $1 + 3(k - 1) + 2\binom{k-1}{2} = k^2$ is correct.

Now, we are ready to show that $|\pi\rangle$ is indeed the eigenstate of \mathcal{L}_k with zero energy. Let's act \mathcal{L}_k on $|\pi\rangle$. One kind of term coming from \mathcal{P} is:

$$\mathcal{P}|\pi\rangle \supset \left(\left(\begin{array}{c} \text{---} \\ \text{---} \end{array} \right) = N \cdot \left(\begin{array}{c} \text{---} \\ \text{---} \end{array} \right) = N|\pi\rangle, \# = k \quad (3.5)$$

Here, to simplify the diagram like (3.4), we use black lines to indicate the links that are relevant for calculation, and a gray background to represent the other links that are not involved in this step of the calculation.

The number of such terms is $\# = k$. So, this contribution cancels the $-k$ constant part in \mathcal{L}_k . The other terms in \mathcal{P} look like:

$$\mathcal{P}|\pi\rangle \supset \left(\left(\begin{array}{c} \text{---} \\ \text{---} \end{array} \right) = \left(\begin{array}{c} \text{---} \\ \text{---} \end{array} \right), \mathcal{P}|\pi\rangle \supset \left(\left(\begin{array}{c} \text{---} \\ \text{---} \end{array} \right) = \left(\begin{array}{c} \text{---} \\ \text{---} \end{array} \right), \# = k^2 - k \quad (3.6)$$

They are canceled by the action of \mathcal{X} and $\bar{\mathcal{X}}$:

$$\mathcal{X}|\pi\rangle \supset \left(\begin{array}{c} \diagup \\ \diagdown \end{array} \right) = \left(\begin{array}{c} \diagdown \\ \diagup \end{array} \right), \quad \bar{\mathcal{X}}|\pi\rangle \supset \left(\begin{array}{c} \diagdown \\ \diagup \end{array} \right) = \left(\begin{array}{c} \diagup \\ \diagdown \end{array} \right), \quad \# = \binom{k}{2} + \binom{k}{2} = k^2 - k \quad (3.7)$$

We notice that the number of terms matches. Putting everything together, this shows that $\mathcal{L}_k|\pi\rangle = 0$.

We notice that the set of ground states $\{|\pi\rangle|\pi \in \mathbb{S}^k\}$ are not orthogonal. In fact, if we define their Gram matrix as $g_{\sigma\tau} = \langle\sigma|\tau\rangle = N^{\ell(\sigma\tau^{-1})}$ ($\ell(\sigma\tau^{-1})$ counts the number of cycles in permutation element $\sigma\tau^{-1}$) and denote its (pseudo)inverse matrix as $g^{\sigma\tau}$ ($g^{\sigma\tau}$ is exactly the Weingarten function $\text{Wg}(\sigma, \tau)$ [56–60]), then the ground state manifold projector $\mathcal{P}_{\text{GS}}^{(k)}$ is given by:

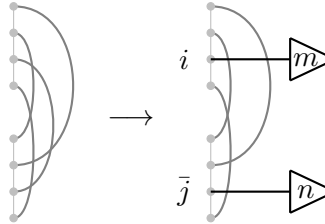
$$\mathcal{U}_k(+\infty) = \mathcal{P}_{\text{GS}}^{(k)} = \sum_{\sigma, \tau \in \mathbb{S}^k} g^{\sigma\tau} |\sigma\rangle\langle\tau| = \int_{\text{Haar}} dU \cdot U^{\otimes k} \otimes U^{*\otimes k} \quad (3.8)$$

This shows that BGUE evolves and saturates to the Haar ensemble at $t = +\infty$.

3.1.2 First excited states

In this section, we explicitly construct the wavefunction of the first excited states and show that their energy is -1 with degeneracy $k \cdot k! \cdot (N^2 - 1)$.

The first excited states are built upon some modifications of the ground state, where one of the links is broken, and two computational basis indices are glued onto the two broken ends. An example for $k = 4$ is:



$$\equiv |mn, i\bar{j}, \pi\rangle, \quad \pi \in \mathbb{S}^{k-1}, \quad m, n = 1, 2, \dots, N \quad (3.9)$$

where i, \bar{j} label the position of the broken links. Let's act \mathcal{P} on $|mn, i\bar{j}, \pi\rangle$, and the five kinds of terms (labeled as $\boxed{1}, \boxed{2}, \boxed{3}, \boxed{4}, \boxed{5}$) are recorded in table 1.

Next, we act $\mathcal{X} + \bar{\mathcal{X}}$ on $|mn, i\bar{j}, \pi\rangle$, and the four kinds of terms (labeled as $\boxed{2'}, \boxed{3'}, \boxed{5.1'}, \boxed{5.2'}$) are recorded in table 2.

We notice that $\boxed{2}$ cancels $\boxed{2'}$, $\boxed{3}$ cancels $\boxed{3'}$, and $\boxed{5}$ cancels $\boxed{5.1'} + \boxed{5.2'}$. Therefore, the surviving terms are $\boxed{1}$ and $\boxed{4}$.

Grouping everything together, we obtain:

$$\begin{aligned} \mathcal{L}_k|mn, i\bar{j}, \pi\rangle &= -k|mn, i\bar{j}, \pi\rangle + N^{-1}(k-1) \cdot N|mn, i\bar{j}, \pi\rangle + N^{-1}\delta_{mn} \sum_{n'=1}^N |n'n', i\bar{j}, \pi\rangle \\ &= -|mn, i\bar{j}, \pi\rangle + N^{-1}\delta_{mn}|\pi'\rangle \end{aligned} \quad (3.10)$$

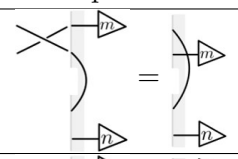
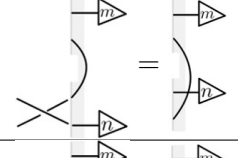
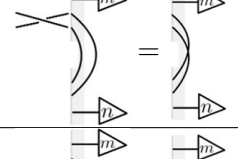
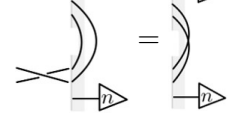
Label	Equation	#
$2'$		$k - 1$
$3'$		$k - 1$
$5.1'$		$\binom{k-1}{2}$
$5.2'$		$\binom{k-1}{2}$

Table 2. $(\mathcal{X} + \bar{\mathcal{X}}) |mn, i\bar{j}, \pi\rangle$ is grouped into four categories. Notice that the total number of terms is $2(k-1) + 2\binom{k-1}{2} = 2\binom{k}{2}$, which is correct.

Notice that $|\pi'\rangle \equiv \sum_{n'=1}^N |n'n', i\bar{j}, \pi\rangle$, $\pi' \in \mathbb{S}^k$ belongs to the ground state manifold. Therefore, we may consider a linear superposition to get rid of this term. Define α to be an $N \times N$ coefficient matrix:

$$|\alpha, i\bar{j}, \pi\rangle \equiv \sum_{m,n=1}^N \alpha_{mn} |mn, i\bar{j}, \pi\rangle \quad (3.11)$$

Then we have:

$$\mathcal{L}_k |\alpha, i\bar{j}, \pi\rangle = -|\alpha, i\bar{j}, \pi\rangle + N^{-1} \text{tr}[\alpha] \cdot |\pi'\rangle \quad (3.12)$$

We see that by choosing α to be traceless, namely $\text{tr}[\alpha] = 0$, we obtain that $\mathcal{L}_k |\alpha, i\bar{j}, \pi\rangle = -|\alpha, i\bar{j}, \pi\rangle$. So we successfully construct the first excited states with eigenvalue -1 .

Next, we aim to determine the degeneracy of the first excited states. There are $N^2 - 1$ choices for the traceless $N \times N$ matrix α , k^2 choices for the positions of m, n located at $i, \bar{j} = 1, 2, \dots, k$, and $(k-1)!$ choices for $\pi \in \mathbb{S}^{k-1}$. Therefore, we may conclude that the degeneracy is $k \cdot k! \cdot (N^2 - 1)$.

We need to show that they are linearly independent. To do so, we analyze the inner product $\langle \alpha', i'\bar{j}', \pi' | \alpha, i\bar{j}, \pi \rangle$ in the large N limit. We first notice that when $(i', \bar{j}') \neq (i, \bar{j})$ or $\pi' \neq \pi$, the inner product is at most $O(N^{k-2})$. But for $(i', \bar{j}') = (i, \bar{j})$ and $\pi' = \pi$, the inner product is of order $O(N^{k-1})$. This shows the Gram matrix is almost block diagonal in the infinite N limit. So, the states with $(i', \bar{j}') \neq (i, \bar{j})$ or $\pi' \neq \pi$ persist to be linearly independent in large but finite N by continuity. Next, we consider the inner product within each block:

$$\langle \alpha', i'\bar{j}, \pi | \alpha, i\bar{j}, \pi \rangle = N^{k-1} \text{tr}[\alpha'^\dagger \alpha] \quad (3.13)$$

This is a standard inner product for traceless matrices. So, there are indeed $N^2 - 1$ linearly independent choices of α .

In summary, this shows that the degeneracy is indeed $k \cdot k! \cdot (N^2 - 1)$ at large but finite N . We expect that some null states will appear if k is of order $O(N)$, which reduces degeneracy. This also happens in the ground state manifold, whose degeneracy starts to decrease from $k!$ when $k > N$ [74].

3.1.3 Second excited states

In this section, we study the family of second excited states of \mathcal{L}_k . The energy spectrum splits into $-2, -2 \pm 2N^{-1}$, and their corresponding degeneracy is summarized in table 4.

Similarly, the second excited states are constructed by breaking two links of ground states. An example for $k = 4$ is given by:

$$\rightarrow \begin{array}{c} i_1 \rightarrow m \\ i_2 \rightarrow n \\ \bar{j}_1 \rightarrow p \\ \bar{j}_2 \rightarrow q \end{array} \equiv |mnpq, i_1 i_2 \bar{j}_1 \bar{j}_2, \pi\rangle, \quad \pi \in \mathbb{S}^{k-2}, \quad m, n, p, q = 1, 2, \dots, N \quad (3.14)$$

where $i_1, i_2, \bar{j}_1, \bar{j}_2 = 1, 2, \dots, k$ label the position of broken links.

Let's act \mathcal{L}_k on $|mnpq, i_1 i_2 \bar{j}_1 \bar{j}_2, \pi\rangle$. From the experience in ground states and first excited states, we see that the following two kinds of terms in \mathcal{P} will cancel those in $\mathcal{X} + \bar{\mathcal{X}}$: (1) exchange the ends of two unbroken links; (2) exchange the ends of one unbroken link and one broken link. So, the terms that are not canceled are the following four kinds of terms (labeled as $\boxed{1''}, \boxed{2''}, \boxed{3''}, \boxed{4''}$) recorded in table 3.

Putting everything together, we obtain:

$$\begin{aligned} \mathcal{L}_k |mnpq, i_1 i_2 \bar{j}_1 \bar{j}_2, \pi\rangle &= -2|mnpq, i_1 i_2 \bar{j}_1 \bar{j}_2, \pi\rangle - N^{-1}|nmpq, i_1 i_2 \bar{j}_1 \bar{j}_2, \pi\rangle - N^{-1}|mnqp, i_1 i_2 \bar{j}_1 \bar{j}_2, \pi\rangle \\ &+ \delta_{mp} \sum_{m'=1}^N |m'nm'q, i_1 i_2 \bar{j}_1 \bar{j}_2, \pi\rangle + \delta_{mq} \sum_{m'=1}^N |m'npm', i_1 i_2 \bar{j}_1 \bar{j}_2, \pi\rangle \\ &+ \delta_{np} \sum_{n'=1}^N |mn'n'q, i_1 i_2 \bar{j}_1 \bar{j}_2, \pi\rangle + \delta_{nq} \sum_{n'=1}^N |mn'pn', i_1 i_2 \bar{j}_1 \bar{j}_2, \pi\rangle \end{aligned} \quad (3.15)$$

The four terms on the second and third lines correspond to $\boxed{1''}$ in table 3. From the diagrams, these states have only one broken link, which belongs to the manifold of the first excited states. To construct eigenstates, we need these four terms to vanish. To achieve this, we define a $N \times N \times N \times N$ four-leg tensor α_{mnpq} and define the linear superposition state:

$$|\alpha, i_1 i_2 \bar{j}_1 \bar{j}_2, \pi\rangle = \sum_{m,n,p,q=1}^N \alpha_{mnpq} |mnpq, i_1 i_2 \bar{j}_1 \bar{j}_2, \pi\rangle \quad (3.16)$$

Label	Comes from where?	Equation	#
$1''$	\mathcal{P}		4
$2''$	\mathcal{P}		$k - 2$
$3''$	\mathcal{X}		1
$4''$	$\bar{\mathcal{X}}$		1

Table 3. $(\mathcal{P} - \mathcal{X} - \bar{\mathcal{X}})|mnpq, i_1 i_2 \bar{j}_1 \bar{j}_2, \pi\rangle$ is grouped into four kinds of terms.

Eliminating four terms from $1''$ is equivalent to imposing the following four linear constraints on α_{mnpq} :

$$\sum_{m'=1}^N \alpha_{m'nm'q} = 0, \quad \sum_{m'=1}^N \alpha_{m'npm'} = 0, \quad \sum_{n'=1}^N \alpha_{mn'n'q} = 0, \quad \sum_{n'=1}^N \alpha_{mn'pn'} = 0, \quad (3.17)$$

Then, the equation is reduced to:

$$\begin{aligned} \mathcal{L}_k |\alpha, i_1 i_2 \bar{j}_1 \bar{j}_2, \pi\rangle &= -2 |\alpha, i_1 i_2 \bar{j}_1 \bar{j}_2, \pi\rangle \\ &- N^{-1} \sum_{m,n,p,q=1}^N \alpha_{mnpq} |mnpq, i_1 i_2 \bar{j}_1 \bar{j}_2, \pi\rangle - N^{-1} \sum_{m,n,p,q=1}^N \alpha_{mnpq} |mnpq, i_1 i_2 \bar{j}_1 \bar{j}_2, \pi\rangle \end{aligned} \quad (3.18)$$

To make eigenstates, we need to further require that α is symmetric/anti-symmetric in its first two indices and symmetric/anti-symmetric in its last two indices. So, we obtain:

$$\left\{ \begin{array}{l} \textcircled{1}: \mathcal{L}_k |\alpha, i_1 i_2 \bar{j}_1 \bar{j}_2, \pi\rangle = -(2 - 2N^{-1}) |\alpha, i_1 i_2 \bar{j}_1 \bar{j}_2, \pi\rangle, \quad \alpha_{mnpq} = -\alpha_{nmpq} = -\alpha_{mnpq} \\ \textcircled{2}: \mathcal{L}_k |\alpha, i_1 i_2 \bar{j}_1 \bar{j}_2, \pi\rangle = -(2 + 2N^{-1}) |\alpha, i_1 i_2 \bar{j}_1 \bar{j}_2, \pi\rangle, \quad \alpha_{mnpq} = \alpha_{nmpq} = \alpha_{mnpq} \\ \textcircled{3}: \mathcal{L}_k |\alpha, i_1 i_2 \bar{j}_1 \bar{j}_2, \pi\rangle = -2 |\alpha, i_1 i_2 \bar{j}_1 \bar{j}_2, \pi\rangle, \quad \alpha_{mnpq} = \alpha_{nmpq} = -\alpha_{mnpq} \\ \textcircled{4}: \mathcal{L}_k |\alpha, i_1 i_2 \bar{j}_1 \bar{j}_2, \pi\rangle = -2 |\alpha, i_1 i_2 \bar{j}_1 \bar{j}_2, \pi\rangle, \quad \alpha_{mnpq} = -\alpha_{nmpq} = \alpha_{mnpq} \end{array} \right. \quad (3.19)$$

Next, we need to count the degeneracy. Similar to the case of the first excited states, the inner product with different positions $(i_1 i_2 \bar{j}_1 \bar{j}_2)$ or different π is at most of order

projector. Picking up $\frac{k!}{4}k(k-1)$ factor from the degeneracy of position and permutation, then by evaluating $\text{tr}[P_{\textcircled{1}}]$, we can obtain the full degeneracy, which we summarize in table 4.

Eigenvalue of \mathcal{L}_k	Degeneracy
$-(2 - 2N^{-1})$	$\frac{k!}{4}k(k-1) \times \text{tr}[P_{\textcircled{1}}] = \frac{k!}{4}k(k-1) \times \frac{1}{4}N^2(N+1)(N-3)$
-2	$\frac{k!}{4}k(k-1) \times (\text{tr}[P_{\textcircled{3}}] + \text{tr}[P_{\textcircled{4}}]) = \frac{k!}{4}k(k-1) \times \frac{1}{2}(N^2-4)(N^2-1)$
$-(2 + 2N^{-1})$	$\frac{k!}{4}k(k-1) \times \text{tr}[P_{\textcircled{2}}] = \frac{k!}{4}k(k-1) \times \frac{1}{4}N^2(N-1)(N+3)$

Table 4. Summary of energy and degeneracy for second excited states

3.1.4 General excited states in the infinite N limit

For general highly excited states, it is challenging to exactly solve the wave function, energy, and degeneracy. However, in the infinite N limit, things simplify.

Consider the p^{th} excited states ($p = 0, 1, 2, \dots, k$), whose wave function is similarly constructed by breaking p -links on top of ground states, and then gluing computational basis to broken ends. These states are labeled by $|m_1 \dots m_p n_1 \dots n_p, i_1 \dots i_p \bar{j}_1 \dots \bar{j}_p, \pi\rangle, \pi \in \mathbb{S}^{k-p}$. Action of $N^{-1}(\mathcal{P} - \mathcal{X} - \bar{\mathcal{X}}) \subset \mathcal{L}_k$ on it will generate four kinds of terms analogous to $\boxed{1''}, \boxed{2''}, \boxed{3''}, \boxed{4''}$ in table 3. In the infinite N limit, $\boxed{1''}, \boxed{3''}, \boxed{4''}$ are suppressed by N^{-1} while $\boxed{2''}$ are not. Therefore, $\mathcal{L}_k \approx -k + \boxed{2''}$:

$$\begin{aligned} \lim_{N \rightarrow \infty} \mathcal{L}_k |m_1 \dots m_p n_1 \dots n_p, i_1 \dots i_p \bar{j}_1 \dots \bar{j}_p, \pi\rangle &= [-k + N^{-1}(k-p)N] |m_1 \dots m_p n_1 \dots n_p, i_1 \dots i_p \bar{j}_1 \dots \bar{j}_p, \pi\rangle \\ &= -p |m_1 \dots m_p n_1 \dots n_p, i_1 \dots i_p \bar{j}_1 \dots \bar{j}_p, \pi\rangle \end{aligned} \quad (3.24)$$

So, they are eigenstates with energy $-p$. The degeneracy of these states is counted to be $\binom{k}{p}^2 (k-p)! N^{2p}$.

3.2 Approaching k -design

Given an ensemble \mathcal{E} of unitaries acting on Hilbert space \mathcal{H} with dimension N , we can ask how close \mathcal{E} is to the Haar ensemble. The distance between two ensembles can be measured by comparing their moments. Let X be an operator on k -copies of Hilbert space: $\mathcal{H}^{\otimes k}$. Then define the following *moment map* channel [16]:

$$\Phi_{\mathcal{E}}^{(k)} : X \longrightarrow \mathbb{E}_{U \in \mathcal{E}} \left[\left(U^{\otimes k} \right) X \left(U^{\dagger \otimes k} \right) \right] \quad (3.25)$$

Then we say that \mathcal{E} is an ε -approximated k -design if the distance between two channels $\Phi_{\mathcal{E}}^{(k)}, \Phi_{\text{Haar}}^{(k)}$ is smaller than ε measured in the diamond norm [16]:

$$\|\Phi_{\mathcal{E}}^{(k)} - \Phi_{\text{Haar}}^{(k)}\|_{\diamond} < \varepsilon \quad (3.26)$$

Since the diamond norm is usually hard to calculate, we may use the frame potential:

$$F_{\mathcal{E}}^{(k)} \equiv \mathbb{E}_{U \in \mathcal{E}} \mathbb{E}_{V \in \mathcal{E}} \left| \text{tr} \left(UV^{\dagger} \right) \right|^{2k} \quad (3.27)$$

to bound the diamond norm via the following inequality [16]:

$$\|\Phi_{\mathcal{E}}^{(k)} - \Phi_{\text{Haar}}^{(k)}\|_{\diamond}^2 \leq N^{2k} (F_{\mathcal{E}}^{(k)} - F_{\text{Haar}}^{(k)}) \quad (3.28)$$

The frame potential for the Haar ensemble is given by $F_{\text{Haar}}^{(k)} = k!$. In our BGUE case, we find that:

$$\begin{aligned} F_{\text{BGUE}}^{(k)}(t) &= \mathbb{E}_{U_t, V_t} \text{tr} \left[\left(U_t^{\otimes k} \otimes U_t^{*\otimes k} \right) \cdot \left(V_t^{\otimes k} \otimes V_t^{*\otimes k} \right)^{\dagger} \right] \\ &= \text{tr} \left[\mathcal{U}_k(t) \cdot \mathcal{U}_k(t)^{\dagger} \right] = \text{tr} [\mathcal{U}_k(2t)] = \text{tr} [e^{2t \cdot \mathcal{L}_k}] \end{aligned} \quad (3.29)$$

where we use the fact that $\mathcal{L}_k = \mathcal{L}_k^{\dagger}$ and $\mathcal{U}_k(t)\mathcal{U}_k(t) = \mathcal{U}_k(2t)$. We see that the frame potential only depends on the spectrum and degeneracy of \mathcal{L}_k . Therefore, using the results of ground states, first excited states, and second excited states, we can approximate the frame potential in the long-time limit:

$$\begin{aligned} F_{\text{BGUE}}^{(k)}(t) &= k! + k!k(N^2 - 1)e^{-2t} + k! \frac{k(k-1)}{16} N^2(N+1)(N-3)e^{-(4-4N^{-1})t} \\ &\quad + k! \frac{k(k-1)}{8} (N^2 - 4)(N^2 - 1)e^{-4t} + k! \frac{k(k-1)}{16} N^2(N-1)(N+3)e^{-(4+4N^{-1})t} \\ &\quad + O(e^{-6t}) \end{aligned} \quad (3.30)$$

Neglecting second excited states, we obtain the time for BGUE to approach an ε -approximated k -design is:

$$t_k \geq \frac{1}{2} [\log \varepsilon^{-2} + k \log N + \log(N^2 - 1) + \log k! + \log k] \quad (3.31)$$

The linear-in- k scaling is consistent with the Brownian SYK result [16].

One can also use the result in section 3.1.4 to calculate the frame potential in a certain limit: scaling $N \rightarrow \infty, t \rightarrow +\infty$ while keeping $Ne^{-t} \rightarrow e^{-\tau}$ finite:

$$F_{\text{BGUE}}^{(k)}(t) \longrightarrow \sum_{p=0}^k \binom{k}{p}^2 (k-p)! N^{2p} \cdot e^{-2pt} = k! \sum_{p=0}^k \binom{k}{p} \frac{1}{p!} (N^2 e^{-2t})^p \quad (3.32)$$

Using Laguerre polynomial $L_k(x) = \sum_{p=0}^k \binom{k}{p} \frac{1}{p!} (-x)^p$, we obtain that:

$$F_{\text{BGUE}}^{(k)}(t) \longrightarrow F_{\text{Haar}}^{(k)} \times L_k(-e^{-2\tau}) \quad (3.33)$$

4 Application in classical shadow tomography

4.1 Brief review of classical shadow tomography

The method of classical shadow tomography aims to predict many observables from just a few measurements. The central spirit of this method is: *First do measurement, and then ask questions* [17, 75–77].

An illuminating example is: given an unknown single qubit state ρ , we want to predict the expectation values of all three Pauli observables $\text{tr}[\rho X], \text{tr}[\rho Y], \text{tr}[\rho Z]$ up to error ε by performing as few measurements as possible. The observation is that since X, Y, Z do not

commute, we cannot measure them simultaneously. In other words, if we measure X to high precision with an error smaller than ε (e.g., we perform measurements in the X -eigenbasis), then the error of predicting $\text{tr}[\rho Z]$ would be much larger than ε . Therefore, instead of measuring in the eigenbasis of X, Y, Z many times, we measure in some random directions a few times, so that each measurement can moderately predict all three $\text{tr}[\rho X], \text{tr}[\rho Y], \text{tr}[\rho Z]$.

Now, we are ready to formulate the task and method of classical shadow tomography [17]. Consider we are handed an experimental oracle that can produce an unknown state ρ on an n -qubit Hilbert space. We want to perform some measurements on ρ , and then predict the expectation value $\text{tr}[\rho O_i]$ of a set of M -observables $\{O_1, O_2, \dots, O_M\}$. The idea is similar: we perform some random measurements on ρ . This is achieved by applying a random unitary $U \in \mathcal{E}$ (\mathcal{E} is a pre-designed ensemble of unitaries) on ρ , and then perform measurements on the computational basis, with the measurement result being $b \in \{0, 1\}^{\otimes n}$. We perform such procedures for K times, each time recording a pair (U_i, b_i) .

Define \mathcal{M} to be the measurement channel:

$$\mathcal{M}[\rho] \equiv \sigma \equiv \mathbb{E}_{\hat{\sigma}} \hat{\sigma} \equiv \mathbb{E}_U \sum_b \text{tr}[\rho \hat{\sigma}_{U,b}] \hat{\sigma}_{U,b}, \quad \hat{\sigma}_{U,b} \equiv U^\dagger |b\rangle \langle b| U \quad (4.1)$$

For a tomographically complete channel [17], \mathcal{M} is invertible. Therefore, we obtain:

$$\rho = \mathcal{M}^{-1}[\sigma] = \mathbb{E}_{\hat{\sigma}} \mathcal{M}^{-1}[\hat{\sigma}] \quad (4.2)$$

In practice, we obtain K realizations of $\hat{\sigma}_i \equiv U_i^\dagger |b_i\rangle \langle b_i| U_i$, therefore an unbiased estimation of ρ is by replacing $\mathbb{E}_{\hat{\sigma}}$ by a finite sum:

$$\rho_{\text{est}} = \frac{1}{K} \sum_{i=1}^K \mathcal{M}^{-1}[\hat{\sigma}_i] \quad (4.3)$$

Then we can use ρ_{est} to calculate $\text{tr}[\rho_{\text{est}} O]$, which is an unbiased estimator of $\text{tr}[\rho O]$:

$$o \equiv \text{tr}[\rho O] = \mathbb{E}_{\hat{\sigma}} \text{tr}[O \mathcal{M}^{-1}[\hat{\sigma}]] \equiv \mathbb{E}_{\hat{\sigma}} \hat{o}, \quad o_{\text{est}} = \frac{1}{K} \sum_{i=1}^K \hat{o}_i \quad (4.4)$$

The performance or accuracy of o_{est} is related to the variance of the classical random variable \hat{o} , which is bounded by:

$$\text{Var}[\hat{o}] \leq \mathbb{E}[\hat{o}^2] = \mathbb{E}_U \sum_b \langle b| U \rho U^\dagger |b\rangle \cdot |\langle b| U \mathcal{M}^{-1}[O] U^\dagger |b\rangle|^2 \quad (4.5)$$

Since one wants to define a quantity that quantifies the variance for generic ρ , which only depends on O , not ρ , we can further maximize over ρ or take an average over ρ . Finally, we obtain a max-version or a mean-version of the shadow norm:

$$\begin{aligned} \text{max-version: } \|O\|_{\text{sh}}^2 &\equiv \max_{\rho} \mathbb{E}_U \sum_b \langle b| U \rho U^\dagger |b\rangle \cdot |\langle b| U \mathcal{M}^{-1}[O] U^\dagger |b\rangle|^2 \\ \text{mean-version: } \|O\|_{\text{sh}}^2 &\equiv \text{mean}_{\rho} \mathbb{E}_U \sum_b \langle b| U \rho U^\dagger |b\rangle \cdot |\langle b| U \mathcal{M}^{-1}[O] U^\dagger |b\rangle|^2 \end{aligned} \quad (4.6)$$

We notice that the measurement channel \mathcal{M} and therefore the shadow norm depends on the choice of random unitary ensemble $U \in \mathcal{E}$. Therefore, for a given type of interested O , we need to design \mathcal{E} to make the shadow norm as small as possible, which in turn decreases the number of measurements needed [17]. For example, if O is a Pauli string with length ℓ , and \mathcal{E} is an ensemble of shallow circuits with depth d (one can imagine that for instance every $U \in \mathcal{E}$ is a brick-wall circuit with depth- d , with every local 2-qubit-gate being Haar-random), then there exists an optimal depth $d_*(\ell)$ that minimizes the shadow norm [18, 19]. See [18, 19, 78–82] for more schemes of designing \mathcal{E} and [83–85] for information-theoretical upper/lower bounds that assess the performance of the shadow tomography method.

4.2 Classical shadow tomography using BGUE

In this section, we apply BGUE to the task of classical shadow tomography [17]. We derive explicit analytical results on shadow norm $\|O\|_{\text{sh}}^2(t)$ as a function of t . We observe that an optimal time $t_*(x_o)$ exists as a function of the off-diagonal portion x_o of O , which minimizes the shadow norm. This phenomenon is analogous to the optimal circuit depth $d_*(\ell)$ in the shallow-circuit protocol [18, 19].

Let's start by calculating the measurement channel. The measurement channel acting on the density matrix is defined as:

$$\mathcal{M}_t[\rho] = \mathbb{E}_{U_t} \sum_b \text{tr}[\rho \hat{\sigma}_{U_t, b}] \hat{\sigma}_{U_t, b} = \mathbb{E}_{U_t} \sum_b \langle b|U_t \rho U_t^\dagger|b\rangle \cdot U_t^\dagger|b\rangle\langle b|U_t \quad (4.7)$$

This can be evaluated exactly using our two-replica result in section 2, using the diagrams in equation (2.10). The result is given by:

$$\mathcal{M}_t[\rho] = N^{-1} \text{tr}[\rho] \cdot \mathbb{I} + N^{-1} \beta_o(t)^{-1} \rho_o + N^{-1} \beta_d(t)^{-1} \rho_d \quad (4.8)$$

where ρ_o is the off-diagonal part of ρ and ρ_d is the traceless diagonal part of ρ . The coefficients are given by:

$$\begin{aligned} N^{-1} \beta_o(t)^{-1} &= 2f_2(t) + 4f_4(t) + Nf_5(t) + Nf_7(t) + 2f_8(t) = \frac{1 - e^{-(2+2N^{-1})t}}{N+1} \\ N^{-1} \beta_d(t)^{-1} &= f_1(t) + 2f_2(t) + 2f_3(t) + 4f_4(t) + Nf_5(t) + f_6(t) + Nf_7(t) + 2f_8(t) = \frac{1 + e^{-(2+2N^{-1})t}}{N+1} \end{aligned} \quad (4.9)$$

where $f_i(t)$ is defined in equation (2.15). The inverse channel can be readily calculated:

$$\mathcal{M}_t^{-1}[O] = N^{-1} \text{tr}[O] \cdot \mathbb{I} + \beta_o(t) O_o + \beta_d(t) O_d \quad (4.10)$$

Shadow Norm. Similarly, O_o, O_d are the off-diagonal and traceless diagonal part of O , respectively. Next, we calculate the (mean-version) shadow norm for a traceless Hermitian

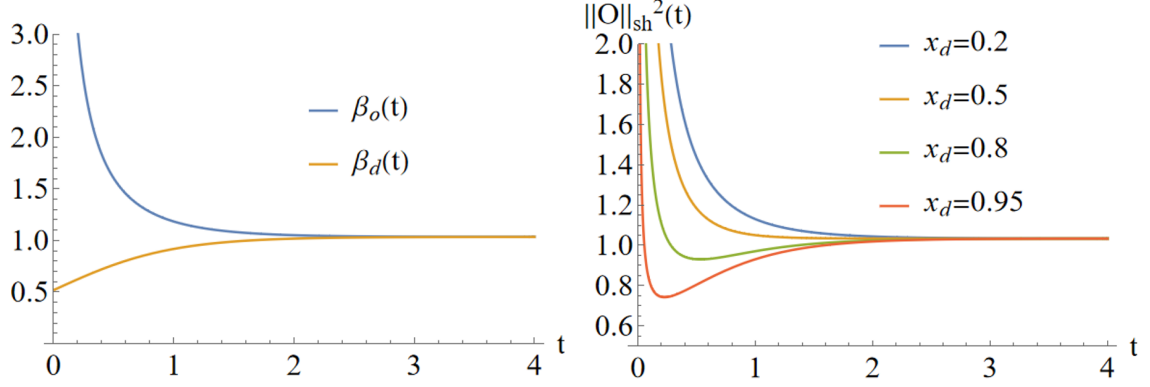


Figure 6. **Left:** Shadow norm for purely diagonal or purely off-diagonal operator. **Right:** Shadow norm (4.12) with mixing diagonal and off-diagonal entry. For both panels, we choose $N = 30$, and the shadow norm is measured in unit of $\|O\|_2^2$.

operator O :

$$\begin{aligned}
\|O\|_{\text{sh}}^2(t) &\equiv \text{mean}_\rho \mathbb{E}_{U_t} \sum_b \langle b|U_t \rho U_t^\dagger|b\rangle \cdot |\langle b|U_t \mathcal{M}_t^{-1}[O]U_t^\dagger|b\rangle|^2 \\
&= N^{-1} \mathbb{E}_{U_t} \sum_b |\langle b|U_t \mathcal{M}_t^{-1}[O]U_t^\dagger|b\rangle|^2 \\
&= N^{-1} \text{tr} (\mathcal{M}_t^{-1}[O] \mathcal{M}_t [\mathcal{M}_t^{-1}[O]]) \\
&= N^{-1} \text{tr} (\mathcal{M}_t^{-1}[O]O) \\
&= \beta_o(t) \text{tr} (O_o^2) + \beta_d(t) \text{tr} (O_d^2) + (\beta_o(t) + \beta_d(t)) \text{tr} (O_o O_d) \\
&= \beta_o(t) \text{tr} (O_o^2) + \beta_d(t) \text{tr} (O_d^2)
\end{aligned} \tag{4.11}$$

where we used the fact that $\text{tr} (O_o O_d) = 0$. Notice that $\text{tr} (O^2) = \text{tr} (O_o^2) + \text{tr} (O_d^2)$. So, we may define x_o, x_d to be the portion of the off-diagonal part and traceless diagonal part inside O : $x_o \equiv \text{tr} (O_o^2) / \text{tr} (O^2)$, $x_d = \text{tr} (O_d^2) / \text{tr} (O^2)$, with the constraint $x_o + x_d = 1$, $x_o, x_d \in [0, 1]$. Thus, the shadow norm in units of the two-norm is given by:

$$\|O\|_{\text{sh}}^2(t) / \|O\|_2^2 = \beta_o(t)x_o + \beta_d(t)x_d = \frac{N+1}{N} \left(\frac{x_o}{1 - e^{-(2+2N^{-1})t}} + \frac{x_d}{1 + e^{-(2+2N^{-1})t}} \right) \tag{4.12}$$

We first analyze the shadow norm of a purely diagonal ($x_d = 1$) or purely off-diagonal operator ($x_o = 1$). We see that $\beta_d(t)$ increases with time. This means that the scrambling will decrease the efficiency of predicting the diagonal operator. On the other hand, $\beta_o(t)$ decreases with time. This means that the scrambling will improve the efficiency of predicting the off-diagonal operator. We notice that $\beta_o(t=0) = +\infty$, which means in the initial time, we cannot predict the off-diagonal operator at all. This is reasonable since without U_t we are just measuring the computational basis, which only knows about the diagonal entries of the operator. We also notice that as $t \rightarrow \infty$, $\beta_o = \beta_d = \frac{N+1}{N}$, approaching the global Haar random result [17]. This is reasonable since Haar randomness is basis independent; therefore, diagonal and off-diagonal should have the same shadow norm. A plot of these phenomena can be found in figure 6.

Optimal Time. Now, we consider O has both O_o and O_d components. It turns out that when $x_d > x_o$, there is an optimal time t_* such that $\|O\|_{\text{sh}}^2(t)$ is minimal:

$$t_*(x_o) = \begin{cases} \frac{1}{2 + 2N^{-1}} \log \left(\frac{1 + \sqrt{1 - (x_d - x_o)^2}}{x_d - x_o} \right), & x_d > x_o \\ +\infty, & x_d \leq x_o \end{cases} \quad (4.13)$$

The minimal shadow norm is given by:

$$\|O\|_{\text{sh}}^2(t_*) / \|O\|_2^2 = \begin{cases} \frac{N+1}{N} \cdot \frac{1}{2} \left[1 + \sqrt{1 - (x_d - x_o)^2} \right], & x_d > x_o \\ \frac{N+1}{N}, & x_d \leq x_o \end{cases} \quad (4.14)$$

This phenomenon is observed in numerical simulations in figure 6. The existence of an optimal time $t_*(x_o)$ as a function of the off-diagonal portion x_o is analogous to the optimal circuit depth $d_*(\ell)$ as a function of the Pauli-string's length ℓ in shallow-circuit classical shadow tomography [18, 19].

5 Conclusion

In this study, we have constructed and thoroughly analyzed the Brownian generalization of the Gaussian Unitary Ensemble (BGUE). Our investigation encompassed both the non-equilibrium dynamics, complexity and test of applications in classical shadow tomography, yielding significant insights into its behavior and potential applications in broaden quantum information tasks.

We began the study of non-equilibrium dynamics in BGUE by deriving explicit analytical expressions for various one-replica and two-replica variables at finite N and t . These variables include the spectral form factor, its fluctuation, the two-point function, the fluctuations of the two-point function, out-of-time-order correlators (OTOC), the second Rényi entropy, and the frame potential for unitary 2-designs.

Our results revealed that BGUE exhibits hyperfast scrambling and the emergence of temperature. Additionally, we identified replica-wormhole-like contributions, leading to a non-decaying two-point function as $t \rightarrow +\infty$ and non-vanishing fluctuations of the two-point function with zero mean value.

We further explored the complexity of BGUE, determining the time required for the ensemble to approximate the Haar ensemble in terms of k -design. Our findings indicate that the timescale is linear in $k \log N$, consistent with previous studies on the Brownian Sachdev-Ye-Kitaev (SYK) model. In our investigation of the low-energy eigen-wavefunctions, spectrum, and degeneracy of the effective imaginary-time evolution operator on $2k$ -replicated contours, we derived long-time results for the frame potential, confirming that the time required for BGUE to reach k -design is linear in k .

In the final section, we applied the BGUE model to classical shadow tomography. We derived analytical results for the shadow norm and identified an optimal time that

minimizes the shadow norm, analogous to the optimal circuit depth in shallow-circuit shadow tomography.

There are some possible interesting questions based on our study of BGUE:

1. *Exact $\mathcal{U}_3(t)$ for three-replica observables.* Many interesting observables need three replicas. One relevant example is the max-version shadow norm defined in (4.6).
2. *Application in other quantum information tasks.* For example, we can study the quantum causal influence (QCI) [86], spacetime entanglement entropy in super-density operator formalism [87], and channel capacity [88]. We are currently exploring these directions.
3. *Adding noise and measurement.* We can add decoherence and measurement to the scrambling of BGUE, which can be used to study Measurement Induced Phase Transition or Noise Induced Phase Transition extensively studied in recent literature.
4. *Brownian generalization of other ensemble.* One direct generalization is consider different symmetry class, like Brownian Gaussian Orthogonal Ensemble (BGOE) and Brownian Symplectic Ensemble (BGSE).

In conclusion, our study provides a comprehensive understanding of the non-equilibrium dynamics and complexity of BGUE, demonstrating its scrambling behavior and potential for its applications in quantum information tasks such as classical shadow tomography. The analytical techniques and results presented here lay a foundation for future explorations of Brownian random matrix models and their applications in quantum physics and beyond.

Acknowledgments

I would like to thank Wanda Hou, Xiao-Liang Qi, Douglas Stanford, Hong-Yi Wang, Jinzhao Wang, Jiuci Xu, Shunyu Yao, Yi-Zhuang You, and Yuzhen Zhang for helpful discussion. I would especially thank Yuzhen Zhang for stimulating conversations on frame potential. I would also thank numerous useful discussions with Hong-Yi Wang on classical shadow tomography. I thank professor Xiao-Liang Qi's support by National Science Foundation under grant No.2111998 and the Simons Foundation.

A Subset of High Energy Spectrum

In this appendix, we aim to gain a deeper understanding of the generic high-energy spectrum of \mathcal{L}_k . Although deriving the general formula for the spectrum and degeneracy by breaking more links on ground states is challenging, we demonstrate a special case where $\{-[p + N^{-1}p(p-1)] | p = 0, 1, \dots, k\}$ is a subset of the spectrum of \mathcal{L}_k , using a different method. To achieve this, we work in an operator basis instead of a state basis.

Consider $B_p^{(k)}$ as an *operator* on the Hilbert space $\mathbb{C}^{\otimes(2kN)}$. $B_p^{(k)}$ is defined by the equal-weight summation of all diagrams with: (1) p -lines connecting upper left and upper right; (2) p -lines connecting lower left and lower right; (3) $(k-p)$ -lines connecting upper

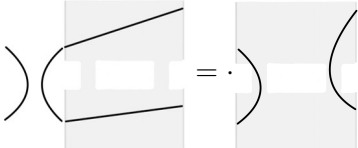
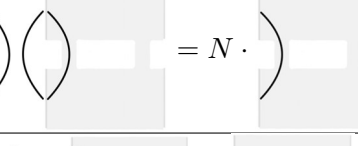

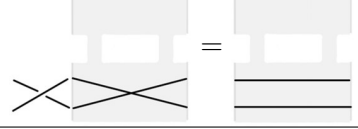
Label	Source	Equation	Count	Mapping of diagrams
$1'''$	\mathcal{P}		p^2	$B_p^{(k)} \rightarrow B_{p-1}^{(k)}$
$2'''$	\mathcal{P}		$k - p$	$B_p^{(k)} \rightarrow B_p^{(k)}$
$3'''$	\mathcal{X}		$\binom{p}{2}$	$B_p^{(k)} \rightarrow B_p^{(k)}$
$4'''$	$\bar{\mathcal{X}}$		$\binom{p}{2}$	$B_p^{(k)} \rightarrow B_p^{(k)}$

Table 5. Action of \mathcal{L}_k on one term in the summand of $B_p^{(k)}$. This table directly corresponds to table 3 row by row.

left and lower left; and (4) $(k-p)$ -lines connecting upper right and lower right. The number of terms in the summand of $B_p^{(k)}$ is:

$$\#(B_p^{(k)}) = \binom{k}{p}^4 [(k-p)!]^2 [p!]^2 \quad (\text{A.1})$$

An example of a diagram within the summand of $B_3^{(6)}$ would be:

$$B_3^{(6)} \supset \left(\begin{array}{c} \text{Diagram with 6 vertical lines on the left and 6 on the right. The left lines are connected by a horizontal line, and the right lines are connected by a horizontal line. A diagonal line connects the top-left to the bottom-right.} \end{array} \right) \quad (\text{A.2})$$

Another example relates to the calculation of the 2-replica case in the previous section 2: $B_0^{(2)} = A_5 + A_7$, $B_1^{(2)} = A_2 + A_4 + A_8$, and $B_2^{(2)} = A_1 + A_3 + A_6$, where A_i is defined in equation (2.10).

Using equation (2.11), we find that $\mathcal{L}_2 B_0^{(2)} = 0$, $\mathcal{L}_2 B_1^{(2)} = -B_1^{(2)} + 4N^{-1} B_0^{(2)}$, and $\mathcal{L}_2 B_2^{(2)} = -(2 + 2N^{-1}) B_2^{(2)} + N^{-1} B_1^{(2)}$. We see that the action of \mathcal{L}_2 is closed in these three bases, which means the vector space defined by $\text{Span}\{B_0^{(2)}, B_1^{(2)}, B_2^{(2)}\}$ forms a three-dimensional representation of \mathcal{L}_2 .

Motivated by this special result at $k = 2$, in this appendix, we show that the linear space $\text{Span}\{B_p^{(k)} | p = 0, 1, \dots, k\}$ forms a $(k + 1)$ -dimensional representation of \mathcal{L}_k . We further show that the representation matrix of \mathcal{L}_k is upper-triangular. Therefore, we can determine the eigenvalues from the diagonal entries of the representation matrix, which turn out to be $\{-[p + N^{-1}p(p - 1)] | p = 0, 1, \dots, k\}$.

Let's act \mathcal{L}_k on $B_p^{(k)}$. The analysis is similar to that in the second excited states, retaining the four terms recorded in table 5.

Therefore, we see that the action of \mathcal{L}_k can either map diagrams in $B_p^{(k)}$ to diagrams in $B_{p-1}^{(k)}$ (process $\boxed{1''''}$), or map diagrams in $B_p^{(k)}$ to diagrams in $B_p^{(k)}$ (processes $\boxed{2''''}$, $\boxed{3''''}$, $\boxed{4''''}$). By the permutation symmetry of \mathcal{L}_k and $B_p^{(k)}$, $B_{p-1}^{(k)}$, we conclude that \mathcal{L}_k takes $B_p^{(k)}$ to be a linear superposition of $B_p^{(k)}$ and $B_{p-1}^{(k)}$:

$$\begin{aligned}
\mathcal{L}_k B_p^{(k)} &= -k B_p^{(k)} + N^{-1} \left(\boxed{1''''} + \boxed{2''''} - \boxed{3''''} - \boxed{4''''} \right) B_p^{(k)} \\
&= -k B_p^{(k)} + N^{-1} p^2 \frac{\#(B_p^{(k)})}{\#(B_{p-1}^{(k)})} \cdot B_{p-1}^{(k)} + N^{-1} (k - p) N \cdot B_p^{(k)} - 2 \times N^{-1} \binom{p}{2} \cdot B_p^{(k)} \\
&= -[p + N^{-1}p(p - 1)] \cdot B_p^{(k)} + N^{-1} (k - p + 1)^2 \cdot B_{p-1}^{(k)}, \quad B_{-1}^{(k)} \equiv 0
\end{aligned} \tag{A.3}$$

This shows that the representation matrix of \mathcal{L}_k is upper-triangular, and therefore we can determine the eigenvalues from the diagonal entries, as claimed at the beginning of this appendix. We also note that when taking $k = 2$, these equations successfully reproduce the two-replica results.

References

- [1] C.-F. Chen, J. Docter, M. Xu, A. Bouland and P. Hayden, *Efficient Unitary T-designs from Random Sums*, [2402.09335](#).
- [2] M. Mehta, *Random Matrices*, ISSN, Elsevier Science (2004).
- [3] J. Cotler, N. Hunter-Jones, J. Liu and B. Yoshida, *Chaos, complexity, and random matrices*, *Journal of High Energy Physics* **2017** (2017) 48.
- [4] D.A. Roberts and B. Yoshida, *Chaos and complexity by design*, *Journal of High Energy Physics* **2017** (2017) 121.
- [5] C.-F. Chen, A. Bouland, F.G.S.L. Brandão, J. Docter, P. Hayden and M. Xu, *Efficient unitary designs and pseudorandom unitaries from permutations*, [2404.16751](#).
- [6] H. Lin and L. Susskind, *Infinite Temperature's Not So Hot*, [2206.01083](#).
- [7] P. Saad, *Late Time Correlation Functions, Baby Universes, and ETH in JT Gravity*, [1910.10311](#).
- [8] J. Maldacena, *Eternal black holes in anti-de sitter*, *Journal of High Energy Physics* **2003** (2003) 021.
- [9] D. Stanford, *More quantum noise from wormholes*, [2008.08570](#).
- [10] C. Dankert, *Efficient simulation of random quantum states and operators*, [quant-ph/0512217](#).

- [11] C. Dankert, R. Cleve, J. Emerson and E. Livine, *Exact and approximate unitary 2-designs and their application to fidelity estimation*, *Phys. Rev. A* **80** (2009) 012304.
- [12] D. Gross, K. Audenaert and J. Eisert, *Evenly distributed unitaries: On the structure of unitary designs*, *Journal of Mathematical Physics* **48** (2007) .
- [13] A. Ambainis and J. Emerson, *Quantum t-designs: t-wise independence in the quantum world*, .
- [14] S. Sachdev, *Bekenstein-hawking entropy and strange metals*, *Phys. Rev. X* **5** (2015) 041025.
- [15] J. Maldacena and D. Stanford, *Remarks on the sachdev-ye-kitaev model*, *Phys. Rev. D* **94** (2016) 106002.
- [16] S.-K. Jian, G. Bentsen and B. Swingle, *Linear growth of circuit complexity from Brownian dynamics*, *JHEP* **08** (2023) 190 [2206.14205].
- [17] H.-Y. Huang, R. Kueng and J. Preskill, *Predicting many properties of a quantum system from very few measurements*, *Nature Physics* **16** (2020) 1050.
- [18] M. Ippoliti, Y. Li, T. Rakovszky and V. Khemani, *Operator relaxation and the optimal depth of classical shadows*, *Phys. Rev. Lett.* **130** (2023) 230403.
- [19] H.-Y. Hu, S. Choi and Y.-Z. You, *Classical shadow tomography with locally scrambled quantum dynamics*, *Phys. Rev. Res.* **5** (2023) 023027.
- [20] S. Guo, M. Sasieta and B. Swingle, *Complexity is not Enough for Randomness*, [2405.17546](#).
- [21] J.S. Cotler, G. Gur-Ari, M. Hanada, J. Polchinski, P. Saad, S.H. Shenker et al., *Black holes and random matrices*, *Journal of High Energy Physics* **2017** (2017) 118.
- [22] J. Maldacena, S.H. Shenker and D. Stanford, *A bound on chaos*, *Journal of High Energy Physics* **2016** (2016) 106.
- [23] Y. Sekino and L. Susskind, *Fast scramblers*, *Journal of High Energy Physics* **2008** (2008) 065.
- [24] D.A. Roberts, D. Stanford and A. Streicher, *Operator growth in the syk model*, *Journal of High Energy Physics* **2018** (2018) 122.
- [25] X.-L. Qi and A. Streicher, *Quantum epidemiology: operator growth, thermal effects, and syk*, *Journal of High Energy Physics* **2019** (2019) 12.
- [26] A. Lucas, *Operator size at finite temperature and planckian bounds on quantum dynamics*, *Phys. Rev. Lett.* **122** (2019) 216601.
- [27] A. Nahum, J. Ruhman, S. Vijay and J. Haah, *Quantum entanglement growth under random unitary dynamics*, *Phys. Rev. X* **7** (2017) 031016.
- [28] A. Nahum, S. Vijay and J. Haah, *Operator spreading in random unitary circuits*, *Phys. Rev. X* **8** (2018) 021014.
- [29] C.W. von Keyserlingk, T. Rakovszky, F. Pollmann and S.L. Sondhi, *Operator hydrodynamics, otocs, and entanglement growth in systems without conservation laws*, *Phys. Rev. X* **8** (2018) 021013.
- [30] P. Hayden, S. Nezami, X.-L. Qi, N. Thomas, M. Walter and Z. Yang, *Holographic duality from random tensor networks*, *Journal of High Energy Physics* **2016** (2016) 9.
- [31] T. Zhou and A. Nahum, *Entanglement membrane in chaotic many-body systems*, *Phys. Rev. X* **10** (2020) 031066.

- [32] M.P.A. Fisher, V. Khemani, A. Nahum and S. Vijay, *Random quantum circuits*, 2022. 10.48550/ARXIV.2207.14280.
- [33] J.M. Koh, S.-N. Sun, M. Motta and A.J. Minnich, *Experimental realization of a measurement-induced entanglement phase transition on a superconducting quantum processor*, 2022.
- [34] Y. Li, Y. Zou, P. Glorioso, E. Altman and M.P.A. Fisher, *Cross entropy benchmark for measurement-induced phase transitions*, 2022. 10.48550/ARXIV.2209.00609.
- [35] B. Skinner, J. Ruhman and A. Nahum, *Measurement-induced phase transitions in the dynamics of entanglement*, *Phys. Rev. X* **9** (2019) 031009.
- [36] M.J. Gullans and D.A. Huse, *Dynamical purification phase transition induced by quantum measurements*, *Phys. Rev. X* **10** (2020) 041020.
- [37] Y. Li, X. Chen and M.P.A. Fisher, *Quantum zeno effect and the many-body entanglement transition*, *Phys. Rev. B* **98** (2018) 205136.
- [38] S.-K. Jian, C. Liu, X. Chen, B. Swingle and P. Zhang, *Measurement-induced phase transition in the monitored sachdev-ye-kitaev model*, *Phys. Rev. Lett.* **127** (2021) 140601.
- [39] C.-M. Jian, Y.-Z. You, R. Vasseur and A.W.W. Ludwig, *Measurement-induced criticality in random quantum circuits*, *Phys. Rev. B* **101** (2020) 104302.
- [40] X. Yu and X.-L. Qi, *Measurement-induced entanglement phase transition in random bilocal circuits*, 2022. 10.48550/ARXIV.2201.12704.
- [41] Y. Li and M.P.A. Fisher, *Statistical mechanics of quantum error correcting codes*, *Phys. Rev. B* **103** (2021) 104306.
- [42] Y. Li, X. Chen and M.P.A. Fisher, *Measurement-driven entanglement transition in hybrid quantum circuits*, *Phys. Rev. B* **100** (2019) 134306.
- [43] C. Noel, P. Niroula, D. Zhu, A. Risinger, L. Egan, D. Biswas et al., *Measurement-induced quantum phases realized in a trapped-ion quantum computer*, *Nature Physics* **18** (2022) 760.
- [44] A. Milekhin and J. Xu, *Revisiting Brownian SYK and its possible relations to de Sitter*, [2312.03623](#).
- [45] D. Stanford, S. Vardhan and S. Yao, *Scramblon loops*, [2311.12121](#).
- [46] D. Stanford, Z. Yang and S. Yao, *Subleading weingartens*, *Journal of High Energy Physics* **2022** (2022) 200.
- [47] Wikipedia contributors, *Partition algebra — Wikipedia, the free encyclopedia*, 2023.
- [48] D.E. Parker, X. Cao, A. Avdoshkin, T. Scaffidi and E. Altman, *A universal operator growth hypothesis*, *Phys. Rev. X* **9** (2019) 041017.
- [49] A. Bhattacharyya, S.S. Haque, G. Jafari, J. Murugan and D. Rapotu, *Krylov complexity and spectral form factor for noisy random matrix models*, *Journal of High Energy Physics* **2023** (2023) 157.
- [50] J. Erdmenger, S.-K. Jian and Z.-Y. Xian, *Universal chaotic dynamics from krylov space*, *Journal of High Energy Physics* **2023** (2023) .
- [51] A. Kar, L. Lamprou, M. Rozali and J. Sully, *Random matrix theory for complexity growth and black hole interiors*, *Journal of High Energy Physics* **2022** (2022) 16.

- [52] C. Liu, H. Tang and H. Zhai, *Krylov complexity in open quantum systems*, *Phys. Rev. Res.* **5** (2023) 033085.
- [53] H. Tang, *Operator Krylov complexity in random matrix theory*, [2312.17416](#).
- [54] H. Tang, *Entanglement entropy in type II_1 von Neumann algebra: examples in Double-Scaled SYK*, [2404.02449](#).
- [55] P. Nandy, A.S. Matsoukas-Roubeas, P. Martínez-Azcona, A. Dymarsky and A. del Campo, *Quantum Dynamics in Krylov Space: Methods and Applications*, [2405.09628](#).
- [56] Wikipedia contributors, *Weingarten function* — *Wikipedia, the free encyclopedia*, 2023.
- [57] B. Collins, S. Matsumoto and J. Novak, *The weingarten calculus*, *Notices of the American Mathematical Society* **69** (2022) 1.
- [58] Y. Gu, *Moments of random matrices and weingarten functions by yinzheng gu*, 2013, <https://api.semanticscholar.org/CorpusID:202611603>.
- [59] L. Zhang, *Matrix integrals over unitary groups: An application of schur-weyl duality*, 2015.
- [60] B. Czech, S. Shuai and H. Tang, *Entropies and reflected entropies in the Hayden-Preskill protocol*, *JHEP* **02** (2024) 040 [[2310.16988](#)].
- [61] G. Penington, S.H. Shenker, D. Stanford and Z. Yang, *Replica wormholes and the black hole interior*, *Journal of High Energy Physics* **2022** (2022) 205.
- [62] A. Almheiri, T. Hartman, J. Maldacena, E. Shaghoulian and A. Tajdini, *Replica wormholes and the entropy of hawking radiation*, *Journal of High Energy Physics* **2020** (2020) 13.
- [63] L. Susskind, *De Sitter Holography: Fluctuations, Anomalous Symmetry, and Wormholes*, *Universe* **7** (2021) 464 [[2106.03964](#)].
- [64] L. Susskind, *Black Holes Hint Towards De Sitter-Matrix Theory*, [2109.01322](#).
- [65] L. Susskind, *Entanglement and Chaos in De Sitter Space Holography: An SYK Example*, *JHAP* **1** (2021) 1 [[2109.14104](#)].
- [66] E. Shaghoulian and L. Susskind, *Entanglement in De Sitter space*, *JHEP* **08** (2022) 198 [[2201.03603](#)].
- [67] L. Susskind, *Scrambling in Double-Scaled SYK and De Sitter Space*, [2205.00315](#).
- [68] L. Susskind, *De Sitter Space, Double-Scaled SYK, and the Separation of Scales in the Semiclassical Limit*, [2209.09999](#).
- [69] L. Susskind, *De Sitter Space has no Chords. Almost Everything is Confined*, [2303.00792](#).
- [70] L. Susskind, *A Paradox and its Resolution Illustrate Principles of de Sitter Holography*, [2304.00589](#).
- [71] A.J. Scott, *Optimizing quantum process tomography with unitary²-designs*, *Journal of Physics A: Mathematical and Theoretical* **41** (2008) 055308.
- [72] N. Hunter-Jones, *Unitary designs from statistical mechanics in random quantum circuits*, 2019.
- [73] F.G. Brandão, W. Chemissany, N. Hunter-Jones, R. Kueng and J. Preskill, *Models of quantum complexity growth*, *PRX Quantum* **2** (2021) 030316.
- [74] P. Saad, S.H. Shenker and D. Stanford, *A semiclassical ramp in syk and in gravity*, 2019.

- [75] A. Elben, S.T. Flammia, H.-Y. Huang, R. Kueng, J. Preskill, B. Vermersch et al., *The randomized measurement toolbox*, *Nature Reviews Physics* **5** (2023) 9.
- [76] H.-Y. Huang, R. Kueng and J. Preskill, *Efficient estimation of pauli observables by derandomization*, *Phys. Rev. Lett.* **127** (2021) 030503.
- [77] H.-Y. Huang, R. Kueng and J. Preskill, *Information-theoretic bounds on quantum advantage in machine learning*, *Phys. Rev. Lett.* **126** (2021) 190505.
- [78] M. Ippoliti and V. Khemani, *Learnability transitions in monitored quantum dynamics via eavesdropper’s classical shadows*, *PRX Quantum* **5** (2024) 020304.
- [79] H.-Y. Hu and Y.-Z. You, *Hamiltonian-driven shadow tomography of quantum states*, *Phys. Rev. Res.* **4** (2022) 013054.
- [80] A.A. Akhtar, H.-Y. Hu and Y.-Z. You, *Scalable and Flexible Classical Shadow Tomography with Tensor Networks*, *Quantum* **7** (2023) 1026.
- [81] A.A. Akhtar, H.-Y. Hu and Y.-Z. You, *Measurement-induced criticality is tomographically optimal*, *Phys. Rev. B* **109** (2024) 094209.
- [82] A.A. Akhtar, N. Anand, J. Marshall and Y.-Z. You, *Dual-unitary classical shadow tomography*, 2024.
- [83] S. Chen, J. Cotler, H.-Y. Huang and J. Li, *A hierarchy for replica quantum advantage*, 2021.
- [84] S. Chen, J. Cotler, H.-Y. Huang and J. Li, *Exponential separations between learning with and without quantum memory*, in *2021 IEEE 62nd Annual Symposium on Foundations of Computer Science (FOCS)*, pp. 574–585, 2022, DOI.
- [85] D. Aharonov, J. Cotler and X.-L. Qi, *Quantum algorithmic measurement*, *Nature Communications* **13** (2022) 887.
- [86] J. Cotler, X. Han, X.-L. Qi and Z. Yang, *Quantum causal influence*, *Journal of High Energy Physics* **2019** (2019) .
- [87] J. Cotler, C.-M. Jian, X.-L. Qi and F. Wilczek, *Superdensity operators for spacetime quantum mechanics*, *Journal of High Energy Physics* **2018** (2018) .
- [88] P. Hosur, X.-L. Qi, D.A. Roberts and B. Yoshida, *Chaos in quantum channels*, *Journal of High Energy Physics* **2016** (2016) .